HSV-1 infection induces a downstream shift of the +1 nucleosome

Elena Weiß[1], Adam W. Whisnant[2,3], Thomas Hennig[2,3], Lara Djakovic[2], Lars Dölken[2,3,4#], Caroline C. Friedel[1#]

[1] Institute of Informatics, Ludwig-Maximilians-Universität München, Amalienstr. 17, 80333 Munich, Germany

[2] Institute for Virology and Immunobiology, Julius-Maximilians-University Würzburg, Versbacher Straße 7, 97078 Würzburg, Germany

[3] Institute for Virology, Medizinische Hochschule Hannover, Carl-Neuberg-Str. 1, 30625 Hannover, Germany

[4] Helmholtz Institute for RNA-based Infection Research (HIRI), Helmholtz-Center for Infection Research (HZI), 97080 Würzburg, Germany

[#] Corresponding authors

E-mail: lars.doelken@uni-wuerzburg.de; Caroline.Friedel@bio.ifi.lmu.de

Abstract

Herpes simplex virus 1 (HSV-1) infection induces a genome-wide loss of host transcriptional activity and widespread disruption of host transcription termination. The latter leads to read-through transcription for thousands of nucleotides beyond poly(A) sites and is associated with the induction of open chromatin downstream of genes. In this study, we show that lytic HSV-1 infection alters chromatin accessibility around host promoters, resulting in an extension of nucleosome-free regions at transcription start sites into downstream regions. This is most prominent for highly expressed genes and still observed upon knockout of the viral immediate-early proteins ICP0, ICP22, and ICP27 and the virion host shutoff protein *vhs*. ChIPmentation analysis of the noncanonical histone variant H2A.Z, which is strongly enriched at +1 and -1 nucleosomes, indicated that the downstream extension of accessible chromatin at promoters is linked to a downstream shift of +1 nucleosomes. In yeast, downstream shifts of +1 nucleosomes are induced by RNA Polymerase II (Pol II) degradation. Accordingly, irreversible depletion of Pol II from genes in human cells using α-amanitin altered H2A.Z occupancy and +1 nucleosome positioning similar to what was observed in lytic HSV-1 infection. Consequently, treatment with phosphonoacetic acid (PAA) and knockout of ICP4, which both prevent viral DNA replication and alleviate the loss of Pol II from host genes, largely abolished the downstream extension of accessible chromatin in HSV-1 infection. In the absence of viral DNA replication, doxycycline-induced expression of ICP27, which redirects Pol II from gene bodies into intergenic regions by disrupting transcription termination, induced an attenuated effect that was further enhanced by co-expression of ICP22. In summary, our study provides strong evidence that HSV-1-induced depletion of Pol II from the host genome leads to a downstream shift of +1 nucleosomes at host gene promoters.

Author Summary

Herpes simplex virus 1 (HSV-1) infection leads to a profound host transcription shutoff during lytic infection. Loss of RNA Polymerase II (Pol II) in yeast has previously been shown to relax +1 nucleosome positioning to more thermodynamically favorable sites downstream of transcription start sites. In this study, we show that a similar phenomenon is likely at play in lytic HSV-1 infection. Sequencing of accessible chromatin revealed a widening of nucleosome-free regions at host gene promoters into downstream regions. By mapping genome-wide positions of the noncanonical histone variant H2A.Z enriched at +1 and -1 nucleosomes, we demonstrate a downstream shift of +1 nucleosomes for most cellular genes in lytic HSV-1 infection. We confirm that the chemical depletion of Pol II from genes leads to a downstream shift of +1 nucleosomes in human cells. Thus, changes in chromatin architecture at promoters in HSV-1 infection are likely a consequence of HSV-1-induced loss of Pol II activity from the host genome.

Introduction

Herpes simplex virus 1 (HSV-1) is one of nine human herpesviruses, and more than half of the global population are latently infected with HSV-1 (1-4). HSV-1 does not only cause the common cold sores but is also responsible for life-threatening diseases, particularly in the immunocompromised (5). The HSV-1 genome consists of 152 kilobases (kb) of double-stranded DNA and encodes for at least 121 large open reading frames (ORFs) and >100 small ORFs (6). Upon lytic infection, four of the five viral immediate early (IE) genes, i.e., ICP0, ICP4, ICP22 and ICP27, hijack the host gene expression machinery to ensure viral replication during early stages of infection (7-11). This results in the recruitment of RNA polymerase II (Pol II) from the host chromatin to viral genomes and a general shutoff of host transcription (7, 9, 11-13). Pol II recruitment to viral genomes is predominantly facilitated by the viral IE protein ICP4 (13), which effectively sequesters Pol II into the viral replication compartments (14). However, ICP4 already depletes Pol II from cellular promoters as early as 2 h post-infection (p.i.), i.e., before the onset of viral genome replication, and independent of viral genome copy number (13). The global host transcription shutoff is further exacerbated by ICP22-mediated inhibition of host transcription elongation (15) and the viral *vhs* (virion host shutoff) protein. *vhs* is a nuclease delivered by the tegument of the incoming viral particles that cleaves both viral and host mRNAs (16-18). We recently demonstrated that *vhs* continuously degrades about 30 % of host mRNAs per hour during the first 8 h of high multiplicity lytic infection of primary human fibroblasts (19).

HSV-1 further disturbs host transcription by inducing a widespread disruption of host transcription termination (DoTT) resulting in read-through transcription for tens of thousands of nucleotides (nt) beyond cellular polyadenylation (pA) sites (20). Read-through transcription commonly extends into downstream genes, leading to a seeming transcriptional induction of

these genes. DoTT negatively affects host gene expression in two ways: First, as read-through transcripts are not exported (21), DoTT prevents the translation of newly transcribed mRNAs and thus dampens the host transcriptional response to infection. Second, it redirects a large fraction of ongoing Pol II transcription from host gene bodies into downstream intergenic regions and, thus, further exacerbates the depletion of Pol II from host genes. We recently showed that ICP27 is sufficient for inducing DoTT (22). Interestingly, transcription downstream of genes (DoG) is also induced in cellular stress responses (21, 23-25). Accordingly, infection with an ICP27-null mutant still induces read-through transcription, albeit at much lower levels, presumably due to a virus-induced cellular stress response (26). In contrast to stress-induced DoGs, HSV-1-induced DoTT is associated with a massive increase of chromatin accessibility downstream of genes (denoted as downstream open chromatin regions (dOCRs)) detectable by ATAC-seq (Assay for Transposase-Accessible Chromatin using sequencing) (21). dOCR induction requires strong absolute levels of transcription downstream of genes, thus it is predominantly observed for highly transcribed genes with strong read-through. Treatment with phosphonoacetic acid (PAA) during HSV-1 infection, which inhibits viral DNA replication (27, 28), results in increased dOCR induction (29). As viral DNA redirects Pol II from the host chromatin, PAA treatment mitigates the loss of Pol II from the host genome and thus increases absolute levels of transcription on host genes and – importantly for dOCR induction – read-through regions. We recently showed that ICP22 is both required and sufficient for inducing dOCRs in the presence of ICP27-induced read-through (29).

As we previously only investigated chromatin accessibility *downstream* of genes, we now further explore our previously published ATAC-seq data to examine changes in chromatin accessibility around host gene promoters. This revealed a broadening of open chromatin regions at promoters into regions downstream of the transcription start sites (TSS) for most host genes. While it was consistently observed in the absence of ICP0, ICP22, ICP27, and *vhs*, PAA

treatment and ICP4 knockout, both of which inhibit viral DNA replication and alleviate the HSV-1-induced loss of host transcription, substantially reduced the extension of open chromatin at the TSS. Weiner *et al.* previously showed that Pol II depletion in yeast induces downstream shifts of +1 nucleosomes, in particular for highly expressed genes (30). Transcribing Pol II disturbs histone-DNA interactions and, at high transcription rates, leads to eviction of nucleosomes from the chromatin (31). Weiner *et al.* proposed that Pol II depletion relaxes chromatin, allowing nucleosomes to shift to more thermodynamically favorable sites. The noncanonical histone H2A variant H2A.Z is strongly enriched at gene promoters at +1 and -1 nucleosome positions (32, 33), likely as H2A.Z deposition increases nucleosome mobility and makes DNA more accessible to the transcriptional machinery (34). We thus performed ChIPmentation for H2A.Z during lytic HSV-1 infection to map +1 nucleosome positions. This showed that changes in chromatin accessibility in HSV-1 infection reflected a downstream shift of +1 nucleosomes. We observed similar changes in H2A.Z occupancy upon treatment with α-amanitin, a deadly toxin found in Amanita mushrooms, which inhibits transcription by preventing translocation of Pol II and triggering degradation of Rpb1, the largest subunit of Pol II (35). Our findings thus provide strong evidence that depletion of Pol II from host genes during HSV-1 infection leads to the downstream shift of +1 nucleosomes to more thermodynamically favorable sites.

Results

Widespread extension of chromatin-free regions downstream of transcription start sites

To investigate changes in chromatin accessibility within promoter regions during HSV-1 infection, we re-analyzed our recently published ATAC-seq data (29) for mock and wild-type (WT) HSV-1 infection of human fetal foreskin fibroblasts (HFF) as well as infection with null mutant viruses for the HSV-1 IE proteins ICP0, ICP22, and ICP27 as well as the tegument-delivered late protein *vhs*. Samples for mock, WT, Δ*vhs*, and ΔICP27 infection were collected at 8 h p.i., while samples for ΔICP0 and ΔICP22 infection were collected at 12 h p.i. To assess chromatin accessibility changes in promoter regions, we identified genomic regions with differential ATAC-seq read density using our recently published RegCFinder method (36). RegCFinder searches for genomic subregions for which the read distribution differs between two conditions (e.g., mock and WT infection). It is targeted towards regions of interest by specifying genomic windows as input (**Sup. Fig 1a** in **S1 File**). For each input window, subregions that show differences in the distribution of reads within this window are identified. Statistical significance and log2 fold-changes for identified subregions are determined by DEXSeq (37). We defined the windows of interest as the ± 3kb promoter region around the TSS of 7,649 human genes. These TSSs were previously defined in our analysis of promoter-proximal Pol II pausing in HSV-1 WT infection (38) based on a re-analysis of published precision nuclear run-on sequencing (PRO-seq) and PROcap-seq (a variation of PRO-seq) data of flavopiridol-treated uninfected HFF. Inhibition of the CDK9 subunit of the positive transcription elongation factor b (P-TEFb) by flavopiridol arrests Pol II in a paused state at the TSS, allowing the mapping of Pol II initiation sites with both PRO- and PROcap-seq. Filtering for high-confidence TSSs confirmed by both data sets and within a maximum distance of 500 bp to the nearest annotated gene on the same strand identified the major TSS for 7,649 genes. Using these 6 kb promoter windows as input, we applied RegCFinder to our ATAC-seq data

for WT and all null-mutant infections in comparison to mock to identify promoter subregions that show differences in the distribution of open chromatin between infection and mock.

It should be noted that dOCRs can extend into downstream genes following very strong read-through transcription. We nevertheless did not filter promoter windows beforehand to exclude genes for which dOCRs extended from an upstream gene into their promoter window for two reasons: (i) Since dOCRs represent changes in chromatin accessibility, RegCFinder should, by design, detect them; (ii) The farther the distance from the upstream gene, the less pronounced are changes in chromatin accessibility in dOCR regions, making it difficult to distinguish them from background. Any approach we tested to filter promoter windows overlapping with dOCRs from upstream genes before the RegCFinder analysis either excluded too many or too few windows. Thus, we decided to first run RegCFinder and then investigate which detected changes were due to the induction of dOCRs from upstream genes.

RegCFinder identified 23,000-24,000 differential subregions (in the following also denoted as RegC, short for regions of change) for each virus infection compared to mock (WT: 23,357 RegC, ΔICP0: 23,532, ΔICP22: 24,640, ΔICP27: 23,523, Δ*vhs*: 23,716, **Sup. Fig 1b** in **S1 File**). Between 29 and 37 % of these showed a statistically significant difference in read density within the corresponding 6 kb promoter windows upon infection (multiple testing adjusted p-value (adj. p.) ≤ 0.01, WT: 8,552 RegC, ΔICP0: 6,740, ΔICP22: 5,710, ΔICP27: 7,188, Δ*vhs*: 6,860). These represented between 3,129 (ΔICP22 infection) and 4,391 (WT) genes (**Sup. Fig 1c** in **S1 File**). The lower fraction of statistically significant differential regions in ΔICP22 infection is likely due to the relatively low number of ATAC-seq reads mapping to the host genome compared to the other infections (~3.8-fold fewer, see **Sup. Table 1** in **S2 File**). The main reason for this was the high fraction of reads mapping to the HSV-1 genome in ΔICP22

infection (70-94%) compared to WT infection (~52%). We confirmed the higher proportion of viral reads in ΔICP22 infection compared to WT in an independent experiment for both 8 and 12 h infection with the ΔICP22 mutant and its parental WT strain F (WT-F, **Sup. Table 1** in **S2 File**).

Fig 1a visualizes the positions of identified RegC for the 4,981 promoter windows containing at least one statistically significant (adj. p. ≤ 0.01) differential region for at least one virus infection compared to mock. Log2 fold-changes for statistically significant regions are illustrated in **Sup. Fig 1d** in **S1 File**. Here, blue indicates that the relative read density in that subregion is increased during virus infection compared to mock (infection>mock, denoted as i-RegC in the following), and red indicates that relative read density in that subregion is higher in mock compared to infection (mock>infection, denoted as m-RegC). Strikingly, our results showed a highly homogeneous picture for WT and null-mutant infections compared to mock, with changes in the same direction observed at approximately the same locations. To identify distinct patterns of changes in chromatin accessibility, we performed hierarchical clustering on the RegC location heatmap in **Fig 1a.** We selected a cutoff on the dendrogram to obtain 14 clusters identified by visual inspection. To visualize the average read density for each cluster, we performed metagene analyses of promoter windows combined with statistics on RegC locations for each cluster (**Fig 1b,d,f,g, Sup. Fig 2** in **S1 File**). Each 6 kb input window was divided into 101 bins of ~59 bp for metagene analyses. For each bin, ATAC-seq read counts were determined, normalized to sequencing depth, normalized to sum up to 1 for each input window, averaged across all windows in each cluster, and then averaged across replicates. In addition, we show which fraction of windows have an m- (red) or i-RegC (blue) for each bin. Based on the location heatmap and the metagene analyses, we identified three major patterns of changes in chromatin accessibility around promoters during WT infection: (I) ATAC-seq peaks at the TSS that shift and/or broaden into regions downstream of the TSS during HSV-1

infection (clusters 1, 2, 4, 5, 9, 10, 12, 14, a total of 3,472 genes, **Fig 1b, Sup. Fig 2a-g** in **S1 File,** examples in **Fig 1c, Sup. Fig 3a-h** in **S1 File**), (II) ATAC-seq peaks at the TSS that shift and/or broaden into regions upstream of the TSS (clusters 6, 7, 11, a total of 919 genes, **Fig 1d, Sup. Fig 2h,i** in **S1 File,** examples in **Fig 1e, Sup. Fig 3i-k** in **S1 File**), and (III) an increase in chromatin accessibility both up- and downstream of the TSS peak in infection compared to mock (cluster 13, 126 genes, **Fig 1f,** example in **Sup. Fig 3l** in **S1 File**). Two clusters (3 and 8, a total of 464 genes) exhibited a combination of patterns I and II with an extension of the TSS peak in both up- and downstream direction (**Fig 1g, Sup. Fig 2j, Sup. Fig 3m,n** in **S1 File**).

Most chromatin accessibility changes at promoters are independent of dOCR induction

First, we evaluated which observed changes were due to dOCRs extending into promoter regions. For this purpose, we determined the fraction of promoter windows in each cluster that overlapped with dOCRs of the 1,296 genes for which we previously showed consistent dOCR induction across different HSV-1 strains (29) (**Fig 2a**). dOCR regions in mock, WT and all null mutant infections (average across two replicates) were identified as previously described (21, 29) (see also Materials and Methods). It is important to note that some relatively short dOCRs are already observed in mock infection, but these substantially extend during HSV-1 infection in read-through regions. In this analysis, we also included ATAC-seq data obtained in the same experiment for 8 h p.i. WT infection combined with PAA treatment (WT+PAA) to identify dOCR regions that are not as clearly detectable without PAA treatment but may still bias promoter analyses. WT (± PAA) and null mutant infections are ordered according to the overall extent of dOCR induction in **Fig 2a**. While no differences to mock infection were observed for ΔICP22 infection as expected, some clusters showed enrichment for dOCR overlaps upon WT(± PAA), ΔICP0, ΔICP27, and Δ*vhs* infection. This increased with the overall extent of dOCR induction in these viruses. Notably, since read-through in ΔICP27 infection is strongly

reduced, dOCR induction is also reduced – but not abolished – as dOCRs require strong read-through transcription.

However, no cluster had more than 20% of promoter windows overlapping with dOCRs even with PAA treatment, and most had <5% overlap, indicating that dOCRs represent only a very small fraction of observed changes in chromatin accessibility around promoters. Most importantly, the extension of accessible chromatin regions at promoters was also observed upon infection with an ICP22-null mutant. Moreover, in contrast to dOCRs, which increase upon PAA treatment, the extension of open chromatin at promoters was strongly reduced by PAA treatment, indicating that it is not linked to dOCRs (**Fig 2b,c**, **Sup. Fig 4-17** in **S1 File**). Even for clusters 12-14, which exhibited some enrichment for dOCRs, most differential regions were also detected in ΔICP22 infection (**Sup. Fig 15-17** in **S1 File**) and thus not linked to dOCR induction. This was confirmed in the independent ATAC-seq experiment for 8 and 12 h infection with WT-F and its ΔICP22 mutant (**Sup. Fig 18**). The absence of ICP0, ICP27, or *vhs* also had little impact on changes in chromatin accessibility around promoters (**Sup. Fig 4-17** in **S1 File**). We conclude that neither dOCR induction nor the activity of ICP0, ICP22, ICP27, or *vhs* alone explains most observed changes in chromatin accessibility at promoters in HSV-1 infection.

Extension of accessible chromatin regions around promoters is linked to transcription

To correlate observed changes to potential transcription factor binding, we next performed motif discovery for novel and known motifs in m- and i-RegC grouped either by cluster or pattern compared to the background of all promoter windows using HOMER (39) but found no enriched motifs. Functional enrichment analysis for Gene Ontology (GO) terms for each cluster also yielded no significant results, except for cluster 13 (pattern III). Cluster 13 was enriched for “mRNA splicing via the spliceosome” and related terms, however, this was mainly due to

several snRNA genes in this cluster. Accordingly, cluster 13 was significantly enriched for snRNA genes (**Fig 2d**, adj. p. = 3×10^{-16}, see Materials and Methods). In contrast, pattern I clusters tended to contain high fractions of protein-coding genes but no or very few snRNAs. Manual investigation of these few snRNAs either showed no shift or an overlap with other protein-coding genes. Thus, most snRNAs either showed no significant changes or a relative increase in chromatin accessibility on both sides of the TSS (= pattern III in cluster 13) but no down- or upstream shifts in chromatin accessibility. Notably, snRNAs are transcribed by RNA Polymerase III (Pol III), not Pol II. However, snRNA loci and other genes not transcribed by Pol II (rRNAs, tRNAs) are repeated several times in the human genome. The quality of read mappings to these loci is thus insufficient to draw a definitive conclusion. Consequently, few snRNA (55), almost no rRNA (12) and no tRNA loci were included in our analysis. In summary, this analysis provides clear evidence for an extension of accessible chromatin at promoters of many genes transcribed by Pol II, particularly protein-coding genes.

Strikingly, cluster 7 (= the most pronounced case of pattern II) was significantly enriched for antisense transcripts (adj. p. = 5×10^{-15}). The other pattern II clusters 6 and 11, as well as cluster 8 (combined pattern I + II), also contained a relatively high fraction of antisense transcripts. Consistently, we found that cluster 7 (adj. p. = 3.8×10^{-14}) and to a lesser degree clusters 6 and 11 (adj. p. = 0.006 and 0.041, respectively) were enriched for bidirectional promoters, i.e., promoters containing an annotated gene start within 1 kb upstream of the TSS of the target gene (= the gene around whose TSS the promoter window was originally defined, **Fig 2e,** see **Fig 1e** for an example). We thus hypothesized that pattern II essentially represented the mirror image of pattern I (mirrored at a vertical axis through the TSS) with the "downstream" broadening/shift of chromatin accessibility occurring in antisense direction for bidirectional promoters. To confirm this, we calculated the sense-to-antisense transcription ratio in promoter windows for all genes. For this purpose, we analyzed RNA-seq data of

chromatin-associated RNA, which depicts nascent transcription, for mock and 8 h p.i. WT HSV-1 infection from our recent study (19). We also included in this analysis the 2,668 genes (denoted as NA group) without significant chromatin accessibility changes that were excluded from **Fig 1a**. Interestingly, metagene analyses for these genes also revealed a slight broadening of the TSS peak into downstream regions. However, this was much less pronounced than for pattern I clusters and, therefore, not detected by RegCFinder (**Sup. Fig 19a** in **S1 File**). To calculate the sense-to-antisense transcription ratio, promoter windows were divided into the regions down- and upstream of the TSS, and expression in chromatin-associated RNA was determined in sense direction for the downstream region (=DSR) and in antisense direction for the upstream region (=UAR). We then compared log2 ratios of DSR to UAR expression between clusters (**Fig 3a)**. Positive log2(DSR:UAR) ratios indicate that sense transcription downstream of the TSS is stronger than antisense transcription upstream of the TSS, and negative values indicate the opposite. Strikingly, all pattern II clusters had significantly lower DSR to UAR ratios than the remaining genes, while pattern I tended to have considerably higher ratios. While for pattern II clusters 6 and 11 median values were still positive, values for cluster 7 with the most pronounced pattern II were commonly negative. Thus, transcription upstream of the TSS in antisense direction was the dominant mode of transcription for cluster 7 promoters, which means pattern II essentially just represents pattern I for the genes on the antisense strand.

Next, we investigated differences in gene expression changes in WT compared to mock infection between patterns (**Sup. Fig 19b** in **S1 File**). This showed a significant difference (adj. $p < 0.001$) for cluster 1, for which gene expression was more strongly down-regulated than for all other genes. No other consistent trends were observed between the different patterns. In contrast, gene expression (quantified as FPKM = fragments per kilobase million mapped reads, **Fig 3b**) differed considerably between patterns. Most pattern I clusters as well as cluster 3

(combined pattern I+II) exhibited median expression levels above average in mock (**Fig 3b**), which was statistically significant for 5 clusters. In contrast, clusters 6, 7 (pattern II) and 8 (combined pattern I+II) exhibited relatively low expression values, with cluster 7 genes having significantly lower expression. The latter is consistent with these genes being less expressed than their antisense counterpart in these bidirectional promoters. Genes without significant chromatin accessibility changes (NA group) also showed significantly lower expression, albeit not as low as cluster 7. These differences between clusters/patterns were generally maintained in HSV-1 infection at lower overall expression levels, consistent with the absence of differences in gene expression fold-changes between most clusters. When stratifying analyzed genes into five equal-sized groups according to FPKM in chromatin-associated RNA in uninfected cells, we observed that the fraction of genes with at least one significant RegC increased with gene expression (**Fig. 3c**). Consistently, pattern II was significantly enriched among the lowliest expressed genes and depleted among genes with medium to high expression (**Fig. 3d**). In contrast, cluster 5, 9 and 10 with pattern I were enriched among the most highly expressed genes. Metagene analyses on the five gene expression groups confirm this trend, with the downstream extension of chromatin accessibility increasing with gene expression (**Fig. 3e-g**). Interestingly, pattern I cluster 1, which showed a significantly higher reduction in gene expression during HSV-1 infection than the other analyzed genes, was most frequent among genes with low to high expression but weakly significantly depleted among the most highly expressed genes. In summary, these results indicate that HSV-1 infection extends the accessible chromatin around promoters in the dominant direction of transcription for most host genes. Here, highly expressed genes and moderately expressed genes with stronger transcription reduction in HSV-1 infection are most strongly affected. Notably, although highly expressed genes do not generally exhibit a stronger reduction of transcription *relative* to their original expression levels in mock, the *absolute* drop in Pol II occupancy between mock and HSV-1 infection is more pronounced than for more lowly expressed genes. Thus, our results show

parallels to observations for yeast that Pol II depletion induces downstream shifts of +1 nucleosomes, which extends nucleosome-free regions and accordingly accessible chromatin at promoters, most prominently for highly expressed genes (30). We thus hypothesized that the loss of Pol II during HSV-1 infection causes the extension of accessible chromatin at promoters during HSV-1 infection.

Changes in chromatin accessibility manifest between 4 and 6 h of HSV-1 infection

To investigate how early in infection changes in chromatin accessibility around promoters can be detected, we ran RegCFinder on an ATAC-seq time-course for 1, 2, 4, 6, and 8 h p.i. WT infection from our previous publication (21) (**Fig 4a,b**). While barely any significant differential regions were identified at 1 and 2 h p.i., 1,963 significant regions in 1,249 promoter windows were identified by 4 h p.i. and 7,558 significant regions in 3,989 promoter windows by 8 h p.i. (**Fig 4b**). Log2 fold-changes for significant differential regions generally reflected the patterns observed in the analysis for WT and null mutant infections (**Fig 4a**). The same applied when we separately determined fold-changes and significance on the time-course data for the differential regions determined for WT vs. mock from our initial analysis (**Sup. Fig 20** in **S1 File**) and when we performed metagene analyses for the clusters from **Fig 1a (Fig 4d-f**, **Sup. Fig 21** in **S1 File**, example genes in **Sup. Fig 22** in **S1 File)**. Although the changes in chromatin accessibility at 8 h p.i. of the time-course were less pronounced than for the original WT vs. mock comparison at 8 h p.i., this nevertheless confirms the changes in chromatin accessibility around promoters in HSV-1 infection in an independent experiment. The lower fraction of viral reads at 8 h p.i. in the time-course experiment (~25%, **Sup. Table 1** in **S2 File**) than for the first WT experiment (~52%) suggests a slower progression of infection in the time-course experiment, which likely explains why the effect was less pronounced.

The time-course analysis also reveals that these changes begin to manifest by 4 h p.i., with 1,249 genes already showing a significant change. Moreover, genes that showed an early effect (by 4 h p.i. or earlier) were significantly more highly expressed than genes that showed an effect by 6 h p.i. or later (**Fig 4c**). The lowest expression was observed for genes with a significant effect in the first WT experiment but not in the time-course. This again confirms the link between expression levels of a gene and the change in chromatin accessibility. Notably, we previously showed that transcriptional activity on host genes drops substantially in the first 4 h of infection to only 40% of transcription in uninfected cells, which was further halved until 8 h p.i. (19). Thus, the onset of the extension of accessible chromatin regions at promoters into downstream (for pattern I) and upstream (for pattern II) regions follows the onset of the drop in host transcription during infection. This provides further evidence for the hypothesis that loss of Pol II from host genes drives changes in chromatin accessibility at promoters. Since the slower progression of virus infection in the time-course experiment likely leads to a less pronounced loss of Pol II from host genes, this would explain the differences in effect between the time-course and the null mutant experiment.

ICP4 knockout reduces, and combined expression of ICP22 and ICP27 induces the extension of accessible chromatin

We already showed above that PAA treatment substantially reduced the broadening and/or downstream shift of accessible chromatin regions at promoters (**Fig 2b,c, Sup. Fig 4-17** in **S1 File**). Since PAA alleviates the depletion of Pol II from host genomes by inhibiting viral DNA replication, this corroborates that Pol II depletion leads to the observed shifts in chromatin accessibility at promoters. The original ATAC-seq experiment with null mutant infections also included infection with an ICP4 null mutant at 8 h p.i., which had not been previously published. Since ICP4 facilitates recruitment of Pol II to viral replication compartments (13, 14), we now also investigated changes in chromatin accessibility in ΔICP4 infection. Strikingly, while we

still observed the extension of accessible chromatin in down- (**Fig 5a**, **Sup. Figs 23a-g,k,l** in **S1 File**) or upstream direction (**Fig 5b**, **Sup Fig. 23h,i** in **S1 File**), it was similarly reduced in ΔICP4 infection compared to WT infection as upon PAA treatment. Interestingly, the fraction of viral reads in ATAC-seq experiments was comparably low at 3-4% in both ΔICP4 and WT+PAA infection (**Sup. Table 1** in **S2 File**), reflecting little viral DNA replication in the absence of ICP4.

We next tested for enrichment in promoter regions of ICP4 binding sites on the human genome previously identified with ChIP-seq by Dremel *et al.* (40). This showed a significant enrichment (adj. p. = 1.1×10^{-5}) of ICP4 binding sites for genes with significant RegC (compared to the NA group of genes without any significant changes) and among these, a weakly significant enrichment in clusters 9 (pattern I, adj. p = 0.0046) and 11 (pattern II, adj. p.=0.0018). Notably, the only cluster with less frequent ICP4 binding than the NA group was cluster 13 (pattern III), which did not show shifts in chromatin accessibility. Thus, promoters of genes with significant shifts in chromatin accessibility are more frequently bound by ICP4 than genes without shifts, providing evidence that Pol II depletion from host genomes by ICP4 contributes to this phenomenon.

ICP27 and ICP22 are still expressed and active in the absence of ICP4, albeit at lower levels, as both read-through transcription and dOCRs are observed in ICP4 null mutants (22). Thus, ICP22 and ICP27 activities still lead to some depletion of Pol II from host gene bodies, which likely explains the residual changes in chromatin accessibility observed in the absence of ICP4. To confirm that ICP27 and/or ICP22 expression alone can induce such changes, we re-investigated our recently published Omni-ATAC-seq (a recent improvement of ATAC-seq (41)) data for telomerase-immortalized human foreskin fibroblasts (T-HFs) that express either

ICP22 (T-HF-ICP22 cells) or ICP27 (T-HF-ICP27 cells) in isolation or combination (T-HF-ICP22/ICP27 cells) upon doxycycline (dox) exposure. While we did not identify any significant RegC upon ICP22 expression alone, ICP27 expression alone led to significant changes for >2,000 genes (**Fig 5c**, **Sup. Fig 24a,b** in **S1 File**). Combined ICP22 and ICP27 expression led to more pronounced results, with the same patterns observed as for WT infection but in an attenuated manner (**Fig 5c-e**, **Fig 24** in **S1 File**). Thus, the combined activity of ICP22 and ICP27 is sufficient to induce a moderate extension of chromatin accessibility at promoters. RNA-seq analysis performed in parallel to ATAC-seq in the same experiment showed that ICP27 was not as strongly expressed in the T-HF-ICP22/ICP27 cells upon dox exposure as in the T-HF-ICP27 cells (~3-fold less). In contrast, ICP22 was much more strongly expressed upon dox exposure in T-HF-ICP22/ICP27 cells than in the T-HF-ICP22 cells (>5-fold more). This indicates that direct effects mediated by ICP22 are important for further extending chromatin accessibility at promoters rather than any indirect effects via enhancement of ICP27 expression and thus read-through.

Nevertheless, our results showed that the pronounced changes observed in WT infection require viral DNA replication but neither ICP22 nor ICP27 expression. Notably, although ICP27 is required for optimal viral DNA replication (42), knockout of ICP27 does not reduce viral DNA replication as effectively as ICP4 knockout or PAA treatment, as ~23% of ATAC-seq reads have a viral origin in ΔICP27 infection (**Sup. Table 1** in **S2 File**). This is comparable to the 8 h p.i. time-point in the time-course experiment. We conclude that the common feature between the different experimental conditions that exhibit promoter chromatin changes is the depletion of RNA Pol II from host promoter regions either by a generalized loss of Pol II or by Pol II translocation into downstream genomic regions upon DoTT.

HSV-1 infection induces a downstream shift of +1 nucleosomes

The HSV-1-induced changes in chromatin accessibility at promoters indicate a broadening of the nucleosome-free region around promoters in either sense (pattern I) or antisense (pattern II) direction. The extension of nucleosome-free regions requires shifts in +1 or -1 nucleosome positions, and depletion of Pol II has been shown to induce a downstream shift of +1 nucleosomes in yeast (30). We, thus, performed ChIPmentation in HFF for mock and WT infection at 8 h p.i. with an antibody recognizing the C-terminal part of the non-canonical histone H2A.Z (n=3 replicates). H2A.Z is highly enriched at gene promoters at -1 and +1 nucleosome positions (32, 33) and is encoded by two genes, whose protein products H2A.Z.1 and H2A.Z.2 differ by only three amino acids. While their genomic occupancy patterns are similar, there are quantitative differences, with H2A.Z.1 being more abundant at active promoters than H2A.Z.2 (43). Since the C-terminal regions of H2A.Z.1 and H2A.Z.2 differ only by the last amino acid, the antibody used for ChIPmentation recognizes both isoforms. A metagene analysis of all analyzed promoter windows showed the expected distribution of H2A.Z occupancy in mock infection with two peaks on both sides of the TSS, corresponding to -1 and +1 nucleosome positions (**Sup. Fig 25a** in **S1 File**).

Application of RegCFinder to H2A.Z ChIPmentation data generally identified a relative increase in H2A.Z downstream of the TSS during infection and a relative decrease upstream of the TSS for pattern I and combined pattern I+II clusters (**Fig 6a**, log2 fold-changes for differential regions shown in **Sup. Fig 25b** in **S1 File**, examples in **Fig 6b**, **Sup. Fig 26a-g,k,l** in **S1 File**). Metagene analyses showed that this reflected a downstream shift and broadening of +1 nucleosome peaks as well as a relative increase of +1 nucleosome peaks compared to -1 nucleosome peaks (**Fig 6d**, **Sup. Fig 25c-i,m,n** in **S1 File**). In contrast, cluster 7 (most pronounced pattern II cluster) showed the opposite trend with relative increases in H2A.Z upstream of the TSS and decreases downstream of the TSS (example in **Fig 6c**). Consistent

with pattern II representing pattern I in antisense direction, the metagene analysis showed an upstream shift and broadening of the -1 nucleosome peak and a relative increase of the -1 nucleosome peak compared to the +1 nucleosome peak (**Fig 6e**). However, this was only observed for a few genes in cluster 6 and cluster 11 (**Fig 6a**, **Sup. Fig 25j,k** in **S1 File**, examples in **Sup. Fig 26h,i** in **S1 File**), which fits with the observation that pattern II in the ATAC-seq data was also much less pronounced for these clusters. In contrast to pattern I and II, pattern III in the ATAC-seq data (cluster 13) was not associated with distribution changes in H2A.Z (**Sup. Fig 25l**, example in **Sup. Fig 26j** in **S1 File**), thus it is not shaped by shifts in +1 and/or -1 nucleosome positioning. This is consistent with pattern III being at least partly associated with dOCR induction for upstream genes, which we previously linked to impaired nucleosome repositioning following Pol II transcription downstream of genes (29).

In summary, our data confirm that the broadening of chromatin accessibility around promoters results from down- and upstream shifts of +1 or -1 nucleosomes, respectively. Here, the shift direction depends on whether sense or antisense transcription represents the dominant direction of transcription at this promoter. Notably, a recent study in yeast proposed that -1 nucleosomes should be considered +1 nucleosomes for antisense transcription (44). This suggests that the loss of Pol II from host promoters during HSV-1 infection induces a shift of +1 and -1 nucleosome positions similar to what was previously observed for yeast. To confirm that inhibition of transcription alone can lead to shifts of +1 and -1 nucleosomes in human cells, we re-analyzed published H2A.Z ChIP-seq data of HCT116 cells with and without α-amanitin treatment from the recent study by Lashgari *et al*. (45). They showed that α-amanitin treatment leads to reduced Pol II levels at gene TSSs and increased incorporation of H2A.Z at TSSs of transcribed genes. Here, Pol II ChIP and RT-qPCR of control genes showed that α-amanitin treatment reduced Pol II signal at the TSS to 10-20% of untreated cells and transcriptional activity to less than 40%. This is not much lower than what has previously been reported for

HSV-1 infection: Abrisch *et al.* found that Pol II occupancy on gene bodies upon 4 h HSV-1 infection was reduced on average to around 20% (9), and we previously estimated that transcriptional activity was reduced to 20-40% between 4 and 8 h p.i. (19). Notably, in contrast to DRB and flavopiridol, which inhibit transcription via arresting Pol II in a paused state at the promoter, α-amanitin induces a loss of Pol II from the host genome, thus making it a better model of HSV-1-induced Pol II depletion.

Lashgari *et al*. previously only analyzed changes in absolute H2A.Z levels at promoters and did not focus on changes in +1 and -1 nucleosome positioning. Metagene and RegCFinder analyses of the H2A.Z ChIP-seq data indeed showed a similar trend upon α-amanitin treatment as during HSV-1 infection (**Fig 6f,g, Sup. Fig 27,** examples are shown in **Sup. Fig 28** in **S1 File**). Pattern I and pattern I+II clusters showed a massive broadening of the +1 nucleosome peak into downstream regions, even more pronounced than what is observed upon HSV-1 infection. In addition, they also exhibited a (less pronounced) broadening of -1 nucleosome peaks. Similarly, pattern II clusters showed a strong broadening of both -1 and +1 nucleosome peaks into upstream regions. In the case of cluster 7 (strongest pattern II), the broadening was much more pronounced for the -1 nucleosome (i.e., the +1 nucleosome in antisense direction) than for the +1 nucleosome (i.e., the -1 nucleosome in antisense direction). This analysis confirms that the depletion of Pol II from promoters leads to a downstream shift of +1 nucleosomes in human cells. In summary, our results demonstrate that the shift of +1 and -1 nucleosomes in the direction of transcription in HSV-1 infection is a consequence of Poll II depletion from host chromatin.

Discussion

Previously, we showed that HSV-1 infection disrupts chromatin architecture downstream of genes with strong read-through transcription. In this study, we reveal that chromatin architecture is also substantially altered at host gene promoters during HSV-1 infection. Here, 57% of genes showed a statistically significant change in the distribution of chromatin accessibility at promoters in WT HSV-1 infection, and metagene analyses indicated similar but less pronounced changes even for genes without statistically significant changes. In essence, we identified three types of changes: Most genes showed a shift and/or broadening of accessible chromatin into regions downstream of the TSS (pattern I). In contrast, ~900 genes showed the opposite trend with a shift and/or broadening of accessible chromatin into regions upstream of the TSS (pattern II). A further ~460 genes exhibited a combination of patterns I and II, with the broadening of accessible chromatin in the downstream direction being more pronounced than in the upstream direction. Only a small set of genes (126 genes) showed relative increases in chromatin accessibility up- and downstream of the TSS, which could partly be attributed to overlaps with dOCRs from upstream genes and partly to an enrichment for short non-coding RNAs not transcribed by Pol II, for which promoter windows were longer than the actual gene. We thus did not further investigate this pattern.

As patterns I and II were still observed in the absence of ICP22, which is necessary for dOCR induction, these are not artifacts of dOCRs extending into downstream genes. On the contrary, PAA treatment, which increases dOCR induction, substantially reduced – though not completely abolished – patterns I and II. Furthermore, knockout of neither ICP0, ICP22, ICP27, nor *vhs* substantially affected patterns I and II. In contrast, ICP4 knockout, similar to PAA treatment, also alleviated the down- and upstream broadening of chromatin accessibility. Both PAA treatment and ICP4 knockout largely abolish viral DNA replication and consequently

alleviate the depletion of Pol II from host genes, leading us to hypothesize that this HSV-1-induced loss of Pol II causes the widespread extension of open chromatin at host gene promoters. This hypothesis was further supported by the observation that combined dox-induced expression of ICP22 and ICP27 (and to a lesser degree dox-induced ICP27 expression alone) led to some broadening of chromatin accessibility at promoters despite knockout of neither of these proteins affecting the HSV-1-induced changes. Knockout of ICP22 or even ICP27 does not sufficiently abolish viral DNA replication and thus has only a minor effect on the depletion of Pol II from host genomes and, consequently, on chromatin accessibility changes. In contrast, in the absence of viral DNA replication, ICP22 and ICP27 (and potentially other viral factors) sufficiently reduce Pol II levels on gene bodies to induce an alleviated form of those chromatin accessibility changes. Notably, we determined that the more pronounced changes upon co-expression of ICP27 with ICP22 compared to expression of ICP27 alone are likely due to the direct effects of ICP22 on transcription. ICP22 interacts with P-TEFb, several transcriptional kinases, as well as elongation factors such as the FACT complex to inhibit transcription elongation of cellular genes (15). Moreover, both the relatively late onset of chromatin accessibility changes between 4 and 8 h p.i. in our time-course ATAC-seq analysis and the generally reduced levels of changes in the time-course, which had a lower fraction of viral reads at 8 h p.i., confirm that significant depletion of Pol II is necessary to observe substantial effects on chromatin accessibility. This also highlights that early (at ~2 h p.i.) ICP4-mediated depletion of Pol II from host promoters before the onset of genome replication does not seem to have a detectable effect.

Analysis of transcriptional activity using RNA-seq of chromatin-associated RNA revealed that pattern I and II are indeed linked to transcription, with pattern I associated with more highly expressed genes and pattern II associated with bidirectional promoters with strong antisense transcription on the opposite strand. In the case of cluster 7, for which pattern II was most

pronounced, antisense transcription was much higher than sense transcription. This was not due to the widespread induction of antisense transcription in HSV-1 infection, which we previously reported on (46), but these genes already exhibited strong transcription in antisense direction in uninfected cells originating from bidirectional promoters. Consistently, cluster 7 was enriched for genes annotated as antisense, and more than a third of these promoters contained an annotated gene starting on the opposite strand within 1 kb upstream of the TSS of the target gene. Thus, pattern II is essentially just pattern I for the genes on the opposite strand in bidirectional promoters.

Since the broadening of chromatin accessibility in promoter regions suggested an extension of nucleosome-free regions at promoters, we mapped +1 and -1 nucleosome positions by ChIPmentation of the H2A.Z histone variant enriched at these nucleosomes. Analysis of H2A.Z occupancy indeed showed a downstream shift of +1 nucleosomes for pattern I genes in HSV-1 infection and an upstream shift of -1 nucleosomes for genes with the most pronounced pattern II (cluster 7). This further confirmed that pattern II just represents pattern I for genes on the antisense strand. It is also consistent with recent results from yeast by Bagchi *et al.* that -1 H2A.Z-containing nucleosomes should be considered as +1 nucleosomes for antisense transcription (44). Downstream shifts of the +1 nucleosome have previously been reported upon Pol II degradation in yeast by Weiner *et al*. (30), in particular for highly expressed genes. Re-analysis of published H2A.Z ChIP-seq data with and without α-amanitin-induced depletion of Pol II from gene promoters confirmed that depletion of Pol II alone is sufficient to induce downstream shifts of +1 nucleosomes in human cells. Moreover, for genes with dominant antisense transcription (cluster 7), it resulted in upstream shifts of -1 nucleosomes. To our knowledge, this is the first study that confirms the effect of Pol II depletion on nucleosome positioning for human cells. The broadening of H2A.Z peaks in both HSV-1 infection and upon α-amanitin treatment, respectively, indicate a less precise positioning of corresponding

nucleosomes. This was more pronounced upon α-amanitin treatment and also observed for -1 nucleosomes, suggesting that loss of Pol II upon α-amanitin treatment is more pronounced than in HSV-1 infection.

One open question remaining concerns the biological significance of the observed changes in nucleosome positioning. Our analysis of gene expression changes did not suggest an effect on differential gene expression, rather the opposite with strong down-regulation leading to the same effect for less strongly expressed genes (cluster 1) as for highly expressed genes that are not more down-regulated than other genes. However, the downstream shifts in +1 nucleosomes may provide an explanation for the downstream shift of Pol II pausing we recently reported for HSV-1 infection (38). The +1 nucleosome was shown to play a role in promoter-proximal Pol II pausing between the promoter and the +1 nucleosome (47). In particular, the +1 nucleosome represents a 2nd barrier to Pol II pause release independent of the main pausing factor negative elongation factor (NELF). Upon NELF depletion, Pol II stops at a 2nd pausing region around the +1 nucleosomal dyad-associated region (48). We previously observed that Pol II pausing in HSV-1 infection is shifted to more downstream and less well-positioned sites for the majority of genes (38), consistent with +1 nucleosome positioning also appearing less well-positioned upon HSV-1 infection in our H2A.Z ChIPmentation data. Alternatively, the shifts in +1 nucleosomes might also be linked to the mobilization of H1, H2 (including H2A.Z), and H4 histones during HSV-1 infection (49-51), which has been proposed to serve as a source of histones for viral chromatin assembly. Nevertheless, even if the changes in nucleosome positioning upon Pol II depletion are of no further functional consequence for HSV-1 infection, they are highly relevant for any functional genomics studies on chromatin architecture in HSV-1 infection or other conditions that deplete Pol II from the genome. If not properly taken into account, the broadening of accessible chromatin at promoters may be mistaken, e.g., for differential transcription factor binding, which could lead to wrong conclusions. Together with

read-through transcription and dOCRs extending into downstream genes, this represents one more example of how HSV-1 infection confounds standard functional genomics analyses. In any case, our study highlights that HSV-1 infection impacts chromatin architecture at promoters independently of the widespread changes downstream of genes mediated by ICP22.

Materials and Methods

Previously published sequencing data analyzed in this study

ATAC-seq for mock and WT HSV-1 infection (strain 17, 8 h p.i.), WT infection with 8 h PAA treatment, infection with ICP0-null mutant (ΔICP0, strain 17, (52), 12 h p.i.), ICP22-null mutant (ΔICP22, R325, strain F, (53), 12 h p.i.), ICP27-null mutant (ΔICP27, strain KOS, (54), 8 h p.i.) and *vhs*-null mutant (Δ*vhs*, strain 17, (55)) in of HFF were taken from our recent publication (29) (n=2 apart from ΔICP22 infection with n=4, GEO accession: GSE185234). This experiment also included infection with an ICP4-null mutant (ΔICP4, n12, strain KOS, (56), 8 h p.i.) which had not previously been published (GEO accession: GSE212820). ATAC-seq data for mock and WT HSV-1 infection of HFF at 1, 2, 4, 6 and 8 h p.i. WT infection (n=2 replicates, GEO accession: GSE100611) and chromatin-associated RNA-seq data for mock and 8 h p.i. WT infection (GEO accession: GSE100576) were taken from our previous publication (21). H2A.Z ChIP-seq data of untreated and α-amanitin-treated HCT116 cells were taken from the study by Lashgari *et al*. (45) (n=2, GEO accession: GSE101427).

ChIPmentation, library preparation and sequencing

HFF were purchased from ECACC and cultured in Dulbecco's Modified Eagle Medium (DMEM, ThermoFisher #41966052) supplemented with 10% (v/v) Fetal Bovine Serum (FBS, Biochrom #S0115), 1× MEM Non-Essential Amino Acids (ThermoFisher #11140050) and 1% penicillin/streptomycin. Two days prior to infection, two million HFF cells were seeded in 15 cm dishes. On the day of infection, cells had expanded to ~80% confluency. Cells were infected

with the respective viruses as described in the results section (n=3). At 8 p.i., cells were fixed for 10 minutes at room temperature by adding 1% formaldehyde (final) directly to the medium. Cells were scraped in 1mL of ice-cold 1x PBS containing protease inhibitor cocktail (1x) (Roche #11836153001) with an additional 1mM phenylmethylsulfonyl fluoride (PMSF). Cells were pelleted at 1500 rpm for 20 min at 4 °C. Supernatant was aspirated and cell pellets were frozen in liquid N_2.

Cell pellets were resuspended in 1.5 mL 0.25% [w/v] SDS sonication buffer (10 mM Tris pH=8.0, 0.25% [w/v] SDS, 2 mM EDTA) with 1x protease inhibitors and 1 mM additional PMSF and incubated on ice for 10 minutes. Cells were sonicated in fifteen 1 minute intervals, 25% amplitude, with Branson Ultrasonics SonifierTM S-450 until most fragments were in the range of 200-700 bp as determined by agarose gel electrophoresis. Two million cells used for the preparation of the ChIPmentation libraries were diluted 1:1.5 with equilibration buffer (10 mM Tris, 233 mM NaCl, 1.66% [v/v] Triton X-100, 0.166% [w/v] sodium deoxycholate, 1 mM EDTA, protease inhibitors) and spun at 14,000x g for 10 minutes at 4 °C to pellet insoluble material. Supernatant was transferred to a new 1.5 mL screw-cap tube and topped up with RIPA-LS (10 mM Tris-HCl pH 8.0, 140 mM NaCl, 1 mM EDTA pH 8.0, 0.1% [w/v] SDS, 0.1% [w/v] sodium deoxycholate, 1% [v/v] Triton X-100, protease inhibitors) to 200 µL. Input and gel samples were preserved. Lysates were incubated with 1µg/IP of anti-H2A.Z antibody (Diagenode, #C15410201) on a rotator overnight at 4 °C.

Dependent on the added amount of antibody, the amount of Protein A magnetic beads (ThermoFisher Scientific #10001D) was adjusted (e.g., for 1-2 µg of antibody/IP = 15 µL of beads) and blocked overnight with 0.1% [w/v] bovine serum albumin in RIPA buffer. On the following day, beads were added to the IP samples for 2 h on a rotator at 4 °C to capture the antibody-bound fragments. The immunoprecipitated chromatin was subsequently washed twice

with 150 µL each of ice-cold buffers RIPA-LS, RIPA-HS (10 mM Tris-HCl pH 8.0, 50 0mM NaCl, 1 mM EDTA pH 8.0, 0.1% [w/v] SDS, 0.1% [v/v] sodium deoxycholate, 1% [v/v] Triton X-100), RIPA-LiCl (10 mM Tris-HCl pH 8.0, 250 mM LiCl, 1 mM EDTA pH 8.0, 0.5% [w/v] sodium deoxycholate, 0.5% [v/v] Nonidet P-40) and 10 mM Tris pH 8.0 containing protease inhibitors. Beads were washed once more with ice-cold 10 mM Tris pH 8.0 lacking inhibitors and transferred into new tubes.

Beads were resuspended in 25 µL of the tagmentation reaction mix (Nextera DNA Sample Prep Kit, Illumina) containing 5 µL of 5x Tagmentation buffer, 1 µL of Tagment DNA enzyme, topped up with H_2O to the final volume and incubated at 37 °C for 10 minutes in a thermocycler. Beads were mixed after 5 minutes by gentle pipetting. To inactivate the Tn5 enzyme, 150 µL of ice-cold RIPA-LS was added to the tagmentation reaction. Beads were washed twice with 150 µL of RIPA-LS and 1x Tris-EDTA and subjected to de-crosslinking by adding 100 µL ChIPmentation elution buffer (160 mM NaCl, 40 µg/mL Rnase A (Sigma-Aldrich #R4642), 1x Tris-EDTA (Sigma #T9285) and incubating for 1h at 37 °C followed by overnight shaking at 65 °C. The next day, 4 mM EDTA and 200 µg/mL Proteinase K (Roche, #03115828001) were added, and samples incubated for another 2h at 45 °C with 1000 rpm shaking. Supernatant was transferred into a new tube and another 100 µL of ChIPmentation elution buffer was added for another hour at 45 °C with 1000 rpm shaking. DNA was isolated with MinElute PCR Purification Kit (Qiagen #28004) and eluted in 21 µL of H_2O.

DNA for the final library was prepared with 25 µL NEBNext Ultra II Q5 Master Mix, 3.75 µL IDT custom primer i5_n_x (10 µM); 3.75 µL IDT custom primer i7_n_x (10 µM); 3.75 µL H_2O and 13.75 µL ChIPmentation DNA. The Cq value obtained from the library quantification, rounded up to the nearest integer plus one additional cycle, was used to amplify the rest of the ChIPmentation DNA. Library qualities were verified by High Sensitivity DNA Analysis on the

Bioanalyzer 2100 (Agilent) before performing sequencing on NextSeq 500 (paired-end 35bp reads) at the Core Unit Systemmedizin, Würzburg, Germany. All samples were sequenced at equimolar ratios.

Read alignment

The read alignment pipeline was implemented and run in the workflow management system Watchdog (57, 58) as already previously described (38). Public sequencing data were downloaded from SRA using the sratoolkit version 2.10.8. Sequencing reads were aligned against the human genome (GRCh37/hg19), the HSV-1 genome (Human herpesvirus 1 strain 17, GenBank accession code: JN555585) and human rRNA sequences using ContextMap2 version 2.7.9 (59) (using BWA as short read aligner (60) and allowing a maximum indel size of 3 and at most 5 mismatches). For the two repeat regions in the HSV-1 genome, only one copy was retained each, excluding nucleotides 1–9,213 and 145,590–152,222 from the alignment. SAM output files of ContextMap2 were converted to BAM files using samtools (61). Read coverage in bedGraph format was calculated from BAM files using BEDTools (62). Subregions of promoter windows (TSS ± 3 kb) with differential read coverage in ATAC-seq and H2A.Z ChIPmentation/-seq data were determined with RegCFinder (36). For this purpose, RegCFinder was applied to ATAC-seq data for all pairwise comparisons of mock to WT and null mutant infections as well as mock to each timepoint of infection for the time-course data and to H2A.Z ChIPmentation and ChIP-seq data for the comparison of mock and WT infection as well as untreated and α-amanitin-treated HCT116 cells.

Quality control

Statistics on numbers of mapped reads and reads mapped to human and HSV-1 genomes were determined with samtools (65). Promoter/Transcript body (PT) scores were determined with ATACseqQC (66). For peak calling, BAM files with mapped reads were converted to BED format using BEDvTools (67) and peaks were determined from these BED files using F-Seq

with default parameters (68). The fraction of reads in peaks (FRiP) was calculated with featureCounts (69) using identified peaks as annotation. Annotation of peaks relative to genes was performed using ChIPseeker (70).

Data plotting and statistical analysis

All figures were created in R and all statistical analyses were performed in R (63). Read coverage plots were created using the R Bioconductor package Gviz (64).

Metagene and clustering analysis

Metagene analyses were performed as previously described (65) using the R program developed for this previous publication (available with the Watchdog *binGenome* module in the Watchdog module repository (https://github.com/watchdog-wms/watchdog-wms-modules/)). For promoter region analyses, the regions −3 kb to +3 kb of the TSS were divided into 101 equal-sized bins for each gene. For each bin, the average coverage per genome position was calculated and bin read coverages were then normalized by dividing by the total sum of all bins. Metagene curves for each replicate were created by averaging results for corresponding bins across all genes in a cluster/group and then averaged across replicates. For hierarchical clustering analysis, RegCFinder profiles of differential regions were calculated for each promoter window and comparison by setting each position in an m-RegC to 1, in an i-RegC to -1 and all other positions to 0. RegCFinder profiles of each promoter window for each comparison were concatenated into one row in the matrix. Hierarchical clustering of the resulting matrix was then performed using the hclust function in R according to Euclidean distances and Ward's clustering criterion.

Analysis of downstream open chromatin regions (dOCRs)

Open chromatin regions (OCRs) were determined from ATAC-seq data by first converting BAM files with mapped reads to BED format using BEDTools (66) and then determining enriched regions from these BED files using F-Seq with default parameters (67). dOCRs for individual genes were calculated from OCRs as previously described (21, 29). In brief, dOCRs are determined for genes by first assigning all OCRs overlapping with the 10 kb downstream of a gene to this gene. Second, OCRs starting at most 5 kb downstream of the so far most downstream OCR of a gene are also assigned to this gene. In both steps, individual OCRs can be assigned to multiple genes. The second step is iterated until no more OCRs can be assigned. The dOCR of a gene is then defined as the region from the gene 3'end to the end of the most downstream OCR assigned to this gene.

Gene expression analysis

Number of fragments (=read pairs) per gene were determined from mapped paired-end RNA-seq reads in a strand-specific manner using featureCounts (68) and gene annotations from Ensembl (version 87 for GRCh37). For genes, all fragments overlapping exonic regions on the corresponding strand by ≥ 25bp were counted for the corresponding gene. Fold-changes in gene expression and statistical significance of changes were determined using DESeq2 (69) and p-values were adjusted for multiple testing using the method by Benjamini and Hochberg (70). Gene expression was quantified in terms of fragments per kilobase of exons per million mapped reads (FPKM). Only reads mapped to the human genome were counted for the total number of mapped reads for FPKM calculation.

Motif discovery and enrichment analysis

Motif discovery was performed for each cluster separately for the i- and m-RegC regions using findMotifsGenome.pl script of the Homer suite (39), with our 7,649 input promoter windows as background. For this purpose, we used the hg19 annotation provided by Homer and automated trimming of input windows was disabled. Significant motifs were identified at a q-value (=False Discovery Rate (FDR) calculated with the Benjamini-Hochberg method (70)) cutoff of 0.01. Over-representation of Gene Ontology (GO) terms was performed separately for each cluster using the g:Profiler webserver (71) and the R package gprofiler2 (72), which provides an R interface to the webserver. As background gene list, the genes corresponding to our 7,649 input promoter windows were provided. P-values were corrected for multiple testing using the Benjamini-Hochberg method (70) and significantly over-represented GO terms were identified at an multiple testing adjusted p-value cutoff of 0.001. Enrichment of gene types (obtained from the Ensembl annotation (version 87 for GRCh37)) within clusters was determined using one-sided Fisher's exact tests (with alternative = greater). Enrichment (odds-ratio >1) or depletion (odds-ratio < 1) of ICP4 binding sites from the study of Dremel *et al.* (40) within clusters as well as enrichment and depletion of clusters within gene groups with different expression levels were determined with two-sided Fisher's exact tests. P-values were always corrected for multiple testing using the Benjamini-Hochberg method.

Acknowledgements

This work was funded by the Deutsche Forschungsgemeinschaft (DFG, German Research Foundation, www.dfg.de) in the framework of the Research Unit FOR5200 DEEP-DV (443644894) project FR 2938/11-1 to C.C.F. and by the European Research Council (ERC, https://erc.europa.eu) project ERC-2021-CoG 101041177 – DecipherHSV to L.D.

References

1. Roizman B KD, RJ W. Herpes Simplex Viruses. In: Knipe DM HP, editor. Fields Virology. 5th. Philadelphia: Lippincott Williams & Wilkins; 2007. p. 2501-601.

2. Pellet PE RB. Herpesviridae. In: Knipe DM HP, editor. Fields Virology. 6th. Philadelphia: Wolters Kluwer Health/Lippincott Williams & Wilkins; 2013. p. 1802-2128.

3. Ablashi D, Agut H, Alvarez-Lafuente R, Clark DA, Dewhurst S, DiLuca D, et al. Classification of HHV-6A and HHV-6B as distinct viruses. Arch Virol. 2014;159(5):863-70.

4. Korr G, Thamm M, Czogiel I, Poethko-Mueller C, Bremer V, Jansen K. Decreasing seroprevalence of herpes simplex virus type 1 and type 2 in Germany leaves many people susceptible to genital infection: time to raise awareness and enhance control. BMC Infect Dis. 2017;17(1):471.

5. Whitley RJ, Roizman B. Herpes simplex virus infections. Lancet. 2001;357(9267):1513-8.

6. Whisnant AW, Jürges CS, Hennig T, Wyler E, Prusty B, Rutkowski AJ, et al. Integrative functional genomics decodes herpes simplex virus 1. Nat Commun. 2020;11(1):2038.

7. Spencer CA, Dahmus ME, Rice SA. Repression of host RNA polymerase II transcription by herpes simplex virus type 1. J Virol. 1997;71(3):2031-40.

8. Rice SA, Davido DJ. HSV-1 ICP22: hijacking host nuclear functions to enhance viral infection. Future Microbiol. 2013;8(3):311-21.

9. Abrisch RG, Eidem TM, Yakovchuk P, Kugel JF, Goodrich JA. Infection by Herpes Simplex Virus 1 Causes Near-Complete Loss of RNA Polymerase II Occupancy on the Host Cell Genome. J Virol. 2015;90(5):2503-13.

10. Dembowski JA, DeLuca NA. Selective recruitment of nuclear factors to productively replicating herpes simplex virus genomes. PLoS Pathog. 2015;11(5):e1004939.

11. Birkenheuer CH, Danko CG, Baines JD. Herpes Simplex Virus 1 Dramatically Alters Loading and Positioning of RNA Polymerase II on Host Genes Early in Infection. J Virol. 2018;92(8).

12. Rivas HG, Schmaling SK, Gaglia MM. Shutoff of Host Gene Expression in Influenza A Virus and Herpesviruses: Similar Mechanisms and Common Themes. Viruses. 2016;8(4):102.

13. Dremel SE, DeLuca NA. Herpes simplex viral nucleoprotein creates a competitive transcriptional environment facilitating robust viral transcription and host shut off. Elife. 2019;8.

14. McSwiggen DT, Hansen AS, Teves SS, Marie-Nelly H, Hao Y, Heckert AB, et al. Evidence for DNA-mediated nuclear compartmentalization distinct from phase separation. eLife. 2019;8:e47098.

15. Isa NF, Bensaude O, Aziz NC, Murphy S. HSV-1 ICP22 Is a Selective Viral Repressor of Cellular RNA Polymerase II-Mediated Transcription Elongation. Vaccines. 2021;9(10):1054.

16. Kwong AD, Frenkel N. Herpes simplex virus-infected cells contain a function(s) that destabilizes both host and viral mRNAs. Proc Natl Acad Sci U S A. 1987;84(7):1926-30.

17. Oroskar AA, Read GS. Control of mRNA stability by the virion host shutoff function of herpes simplex virus. J Virol. 1989;63(5):1897-906.

18. Feng P, Everly DN, Jr., Read GS. mRNA decay during herpesvirus infections: interaction between a putative viral nuclease and a cellular translation factor. J Virol. 2001;75(21):10272-80.

19. Friedel CC, Whisnant AW, Djakovic L, Rutkowski AJ, Friedl MS, Kluge M, et al. Dissecting Herpes Simplex Virus 1-Induced Host Shutoff at the RNA Level. J Virol. 2021;95(3).

20. Rutkowski AJ, Erhard F, L'Hernault A, Bonfert T, Schilhabel M, Crump C, et al. Widespread disruption of host transcription termination in HSV-1 infection. Nat Commun. 2015;6:7126.

21. Hennig T, Michalski M, Rutkowski AJ, Djakovic L, Whisnant AW, Friedl MS, et al. HSV-1-induced disruption of transcription termination resembles a cellular stress response but selectively increases chromatin accessibility downstream of genes. PLoS Pathog. 2018;14(3):e1006954.

22. Wang X, Hennig T, Whisnant AW, Erhard F, Prusty BK, Friedel CC, et al. Herpes simplex virus blocks host transcription termination via the bimodal activities of ICP27. Nat Commun. 2020;11(1):293.

23. Vilborg A, Passarelli MC, Yario TA, Tycowski KT, Steitz JA. Widespread Inducible Transcription Downstream of Human Genes. Mol Cell. 2015;59(3):449-61.

24. Rosa-Mercado NA, Zimmer JT, Apostolidi M, Rinehart J, Simon MD, Steitz JA. Hyperosmotic stress alters the RNA polymerase II interactome and induces readthrough transcription despite widespread transcriptional repression. Mol Cell. 2021;81(3):502-13 e4.

25. Hadar S, Meller A, Saida N, Shalgi R. Stress-induced transcriptional readthrough into neighboring genes is linked to intron retention. iScience. 2022;25(12):105543.

26. Wu N, Watkins SC, Schaffer PA, DeLuca NA. Prolonged gene expression and cell survival after infection by a herpes simplex virus mutant defective in the immediate-early genes encoding ICP4, ICP27, and ICP22. Journal of Virology. 1996;70(9):6358-69.

27. Honess RW, Watson DH. Herpes simplex virus resistance and sensitivity to phosphonoacetic acid. Journal of Virology. 1977;21(2):584-600.

28. Becker Y, Asher Y, Cohen Y, Weinberg-Zahlering E, Shlomai J. Phosphonoacetic Acid-Resistant Mutants of Herpes Simplex Virus: Effect of Phosphonoacetic Acid on Virus Replication and In Vitro Deoxyribonucleic Acid Synthesis in Isolated Nuclei. Antimicrobial Agents and Chemotherapy. 1977;11(5):919-22.

29. Djakovic L, Hennig T, Reinisch K, Milic A, Whisnant AW, Wolf K, et al. The HSV-1 ICP22 protein selectively impairs histone repositioning upon Pol II transcription downstream of genes. Nat Commun. 2023;14(1):4591.

30. Weiner A, Hughes A, Yassour M, Rando OJ, Friedman N. High-resolution nucleosome mapping reveals transcription-dependent promoter packaging. Genome Res. 2010;20(1):90-100.

31. Schwabish MA SK. Evidence for eviction and rapid deposition of histones upon transcriptional elongation by RNA polymerase II. Mol Cell Biol. 2004;24(23):10111-7.

32. Barski A, Cuddapah S, Cui K, Roh TY, Schones DE, Wang Z, et al. High-resolution profiling of histone methylations in the human genome. Cell. 2007;129(4):823-37.

33. Raisner RM, Hartley PD, Meneghini MD, Bao MZ, Liu CL, Schreiber SL, et al. Histone variant H2A.Z marks the 5' ends of both active and inactive genes in euchromatin. Cell. 2005;123(2):233-48.

34. Li S, Wei T, Panchenko AR. Histone variant H2A.Z modulates nucleosome dynamics to promote DNA accessibility. Nature Communications. 2023;14(1):769.

35. Bensaude O. Inhibiting eukaryotic transcription. Which compound to choose? How to evaluate its activity? Transcription. 2011;2(3):103-8.

36. Weiss E, Friedel CC. RegCFinder: targeted discovery of genomic subregions with differential read density. Bioinform Adv. 2023;3(1):vbad085.

37. Anders S RA, Huber W. Detecting differential usage of exons from RNA-seq data. Genome Research. 2012;22(10):2008-17.

38. Weiss E, Hennig T, Grassl P, Djakovic L, Whisnant AW, Jurges CS, et al. HSV-1 Infection Induces a Downstream Shift of Promoter-Proximal Pausing for Host Genes. J Virol. 2023;97(5):e0038123.

39. Heinz S, Benner C, Spann N, Bertolino E, Lin YC, Laslo P, et al. Simple combinations of lineage-determining transcription factors prime cis-regulatory elements required for macrophage and B cell identities. Mol Cell. 2010;38(4):576-89.

40. Dremel SE, Sivrich FL, Tucker JM, Glaunsinger BA, DeLuca NA. Manipulation of RNA polymerase III by Herpes Simplex Virus-1. Nature Communications. 2022;13(1):623.

41. Corces MR, Trevino AE, Hamilton EG, Greenside PG, Sinnott-Armstrong NA, Vesuna S, et al. An improved ATAC-seq protocol reduces background and enables interrogation of frozen tissues. Nature Methods. 2017;14(10):959-62.

42. Uprichard SL, Knipe DM. Herpes simplex ICP27 mutant viruses exhibit reduced expression of specific DNA replication genes. Journal of Virology. 1996;70(3):1969-80.

43. Greenberg RS, Long HK, Swigut T, Wysocka J. Single Amino Acid Change Underlies Distinct Roles of H2A.Z Subtypes in Human Syndrome. Cell. 2019;178(6):1421-36 e24.

44. Bagchi DN, Battenhouse AM, Park D, Iyer VR. The histone variant H2A.Z in yeast is almost exclusively incorporated into the +1 nucleosome in the direction of transcription. Nucleic Acids Research. 2020;48(1):157-70.

45. Lashgari A, Millau J-F, Jacques P-É, Gaudreau L. Global inhibition of transcription causes an increase in histone H2A.Z incorporation within gene bodies. Nucleic Acids Research. 2017;45(22):12715-22.

46. Wyler E, Menegatti J, Franke V, Kocks C, Boltengagen A, Hennig T, et al. Widespread activation of antisense transcription of the host genome during herpes simplex virus 1 infection. Genome Biology. 2017;18(1):209.

47. Jimeno-González S, Ceballos-Chávez M, Reyes JC. A positioned +1 nucleosome enhances promoter-proximal pausing. Nucleic Acids Research. 2015;43(6):3068-78.

48. Aoi Y, Smith ER, Shah AP, Rendleman EJ, Marshall SA, Woodfin AR, et al. NELF Regulates a Promoter-Proximal Step Distinct from RNA Pol II Pause-Release. Molecular Cell. 2020;78(2):261-74.e5.

49. Conn KL HM, Schang LM. Linker histones are mobilized during infection with herpes simplex virus type 1. J Virol. 2008;82:8629–46.

50. Conn KL HM, Schang LM. Core histones H2B and H4 are mobilized during infection with herpes simplex virus 1. J Virol. 2011;85:13234–52.

51. Conn KL, Schang LM. Chromatin Dynamics during Lytic Infection with Herpes Simplex Virus 1. Viruses. 2013;5(7):1758-86.

52. Stow ND, Stow EC. Isolation and Characterization of a Herpes Simplex Virus Type 1 Mutant Containing a Deletion within the Gene Encoding the Immediate Early Polypeptide Vmw110. Journal of General Virology. 1986;67(12):2571-85.

53. Post LE, Roizman B. A generalized technique for deletion of specific genes in large genomes: a gene 22 of herpes simplex virus 1 is not essential for growth. Cell. 1981;25(1):227-32.

54. Smith IL, Hardwicke MA, Sandri-Goldin RM. Evidence that the herpes simplex virus immediate early protein ICP27 acts post-transcriptionally during infection to regulate gene expression. Virology. 1992;186(1):74-86.

55. Fenwick ML, Everett RD. Inactivation of the Shutoff Gene (UL41) of Herpes Simplex Virus Types 1 and 2. Journal of General Virology. 1990;71(12):2961-7.

56. DeLuca NA, Schaffer PA. Physical and functional domains of the herpes simplex virus transcriptional regulatory protein ICP4. Journal of Virology. 1988;62(3):732-43.

57. Kluge M, Friedel CC. Watchdog - a workflow management system for the distributed analysis of large-scale experimental data. BMC Bioinformatics. 2018;19(1):97.

58. Kluge M, Friedl MS, Menzel AL, Friedel CC. Watchdog 2.0: New developments for reusability, reproducibility, and workflow execution. Gigascience. 2020;9(6).

59. Bonfert T, Kirner E, Csaba G, Zimmer R, Friedel CC. ContextMap 2: fast and accurate context-based RNA-seq mapping. BMC Bioinformatics. 2015;16:122.

60. Li H, Durbin R. Fast and accurate short read alignment with Burrows-Wheeler transform. Bioinformatics. 2009;25(14):1754-60.

61. Danecek P, Bonfield JK, Liddle J, Marshall J, Ohan V, Pollard MO, et al. Twelve years of SAMtools and BCFtools. Gigascience. 2021;10(2).

62. Quinlan AR, Hall IM. BEDTools: a flexible suite of utilities for comparing genomic features. Bioinformatics. 2010;26(6):841-2.

63. R Core Team. R: A Language and Environment for Statistical Computing. Vienna, Austria2022.

64. Hahne F, Ivanek R. Visualizing Genomic Data Using Gviz and Bioconductor. Methods Mol Biol. 2016;1418:335-51.

65. Chirackal Manavalan AP, Pilarova K, Kluge M, Bartholomeeusen K, Rajecky M, Oppelt J, et al. CDK12 controls G1/S progression by regulating RNAPII processivity at core DNA replication genes. EMBO Rep. 2019;20(9):e47592.

66. Quinlan AR, Hall IM. BEDTools: a flexible suite of utilities for comparing genomic features. Bioinformatics. 2010;26(6):841-2.

67. Boyle AP, Guinney J, Crawford GE, Furey TS. F-Seq: a feature density estimator for high-throughput sequence tags. Bioinformatics. 2008;24(21):2537-8.

68. Liao Y, Smyth GK, Shi W. featureCounts: an efficient general purpose program for assigning sequence reads to genomic features. Bioinformatics. 2014;30(7):923-30.

69. Love MI, Huber W, Anders S. Moderated estimation of fold change and dispersion for RNA-seq data with DESeq2. Genome Biol. 2014;15(12):550.

70. Benjamini Y HY. Controlling the False Discovery Rate: A Practical and Powerful Approach to Multiple Testing. Journal of the Royal Statistical Society Series B (Methodological). 1995;57(1):289-300.

71. Raudvere U, Kolberg L, Kuzmin I, Arak T, Adler P, Peterson H, et al. g:Profiler: a web server for functional enrichment analysis and conversions of gene lists (2019 update). Nucleic Acids Res. 2019;47(W1):W191-W8.

72. Kolberg L, Raudvere U, Kuzmin I, Vilo J, Peterson H. gprofiler2 -- an R package for gene list functional enrichment analysis and namespace conversion toolset g:Profiler. F1000Res. 2020;9.

Supporting information

S1 File. Supplementary Figures.

Contains Supplementary Figures 1-28 and legends (PDF).

S2 File. Supplementary Tables.

Contains Supplementary Table 1 with statistics on all ATAC-seq samples analyzed for this study (XLSX).

Figures

Fig 1: HSV-1 infection impacts chromatin accessibility around promoters for the majority of host genes.

(a) Heatmap illustrating the location of differential regions (m- and i-RegC) identified by RegCFinder on the ATAC-seq data for WT, ΔICP0, ΔICP22, ΔICP27, and Δ*vhs* infection compared to mock infection. Results are shown for 4,981 (out of 7,649) promoter windows containing at least one statistically significant (adj. p. ≤ 0.01) differential region for at least one virus infection compared to mock. Red and blue colors represent m-RegC (mock>infection) and i-RegC (infection>mock) locations, respectively, within promoter windows. Here, each heatmap row shows results for the same input window in different comparisons of virus

infection to mock. Colored rectangles on top of the heatmap indicate which virus infection was compared to mock. Black vertical lines in the center of each part of the heatmap indicate the position of the TSS. Hierarchical clustering was performed according to Euclidean distances and Ward's clustering criterion, and the cutoff on the hierarchical clustering dendrogram was selected to obtain 14 clusters (marked by colored rectangles between the dendrogram and heatmap and numbered from top to bottom as indicated). Log2 fold-changes for differential regions are shown in **Sup. Fig 1d** in **S1 File. (b)** Metagene plot showing the average ATAC-seq profile around the TSS ± 3 kb in mock (red) and WT (blue) infection for cluster 5, an example for pattern I. For a description of metagene plots, see Materials and Methods. The colored bands below the metagene curves in each panel indicate the percentage of genes having an m- or i-RegC (red or blue, respectively) at that position. **(c)** Read coverage in a ±3.6 kb window around the TSS in ATAC-seq data of mock (red) and WT (blue) infection, for example, gene FBXO28 with pattern I. Read coverage was normalized to the total number of mapped reads for each sample and averaged between replicates. A short vertical line below the read coverage track for mock infection indicates the TSS. Gene annotation is indicated at the top. Boxes represent exons, lines represent introns, and the direction of transcription is indicated by arrowheads. Below the read coverage track for WT infection, m-RegC (red bars) and i-RegC (blue bars) are shown for the comparison of WT vs. mock infection. **(d)** Metagene plot as in **(b)** for cluster 7, the most pronounced case of pattern II. **(e)** Read coverage plot as in **(c)** for example gene ARHGAP1 with pattern II. Here, the promoter window also contains the TSS of the ZNF408 gene on the opposite strand, and the accessible chromatin region is extended upstream of the ARHGAP1 TSS, i.e., downstream of the ZNF408 TSS. **(f,g)** Metagene plots as in **(b)** for **(f)** cluster 13, which exhibits pattern III, and **(g)** cluster 8, one of two clusters exhibiting the combined I+II pattern.

Fig 2: Changes in chromatin accessibility at promoters are mostly independent of dOCR induction.

(a) Bar plots showing the percentage of promoter regions for each cluster overlapping with dOCRs downstream of the 1,296 genes for which we previously showed consistent dOCR induction across different HSV-1 strains (29). dOCR regions in mock, WT (± PAA treatment), and null mutant infection were calculated as previously described (29) (see Materials and Methods for further details), and the overlaps of promoter windows to dOCR regions originating from an upstream gene were determined for each cluster. WT (± PAA treatment) and null mutant infection are ordered according to the overall extent of dOCR induction. Only a few clusters (12-14) showed some enrichment for dOCRs from upstream genes, which was abolished in ΔICP22 infection. **(b-c)** Metagene curves showing average ATAC-seq profiles in promoter windows for mock (red), WT (blue), WT+PAA (green), and ΔICP22 (orange) infection for clusters 5 **(b)** and 7 **(c)**. (**d**) Barplot showing the percentage of genes in each cluster annotated as either protein-coding, long intervening/intergenic noncoding RNAs (lincRNA), snRNA, antisense, or others in Ensembl. The significance of enrichment of each gene type in each cluster was determined using a one-sided Fisher's exact test (with alternative = greater), and p-values were corrected for multiple testing using the Benjamini-Hochberg method. Adj. p. < 0.05 are indicated in the corresponding field of the barplot. (**e**) The percentage of bidirectional promoters in each cluster was calculated as the percentage of promoter windows containing a protein-coding, lincRNA, or antisense gene (according to Ensembl annotation) on the opposite strand to the target gene starting within 1 kb upstream of the TSS of the target gene. Enrichment and significance analysis and multiple testing correction were performed as for (**d**) and adj. p. < 0.05 are indicated on top of bars.

Fig 3: Changes in chromatin accessibility at promoters are linked to transcription.

(a,b) Boxplots showing the distribution of **(a)** log2(DSR:UAR) ratios and **(b)** gene expression (FPKM) values in chromatin-associated RNA in mock (red) and 8 h p.i. WT (blue) HSV-1 infection for all clusters (grouped by pattern, cluster numbers are shown below each boxplot) and remaining genes without significant chromatin accessibility changes (NA group). DSR was calculated as the expression in chromatin-associated RNA for the region downstream of the TSS in the sense direction of the target gene and UAR as the expression in the upstream region in the antisense direction. P-values for Wilcoxon rank sum tests comparing values in mock infection for each cluster against all other analyzed genes are indicated below cluster numbers and were corrected for multiple testing using the Bonferroni method. **(c)** Barplot showing the percentage of genes with very low, low, medium, high and very high gene expression with at least one significant differential region (RegC). Here, gene expression cutoffs for the five groups were determined such that each group contains the same number of genes and are indicated below the labels on the x-axis. Multiple testing corrected p-values for two-sided Fisher's exact tests comparing the fraction of genes with RegC between subsequent gene expression groups are indicated on top of bars. **(d)** Percentage of genes within each cluster among those genes with at least one significant RegC for the five gene expression groups from **(c)**. Significance of enrichment or depletion for each cluster in each gene group was determined with two-sided Fisher's exact tests and multiple testing correction was performed with the method by Benjamini and Hochberg. Adj. p. < 0.05 are shown and are underlined in case the cluster is enriched and not underlined if it is depleted. Clustered are ordered and colored according to pattern (red-yellow: pattern I, green: pattern I + II, blue: pattern II, magenta: pattern III). **(e-g)** Metagene curves showing average ATAC-seq profiles in promoter windows for mock (red) and WT infection (blue) for genes with very low, medium, and very high expression from **(b)**.

Fig. 4: Changes in chromatin accessibility begin to manifest between 4 and 8 h p.i. depending on gene expression

(a) Heatmap showing the log2 fold-changes determined with DEXSeq on the ATAC-seq time-course data (1, 2, 4, 6 and 8 h p.i. WT infection compared to mock infection) for statistically significant differential regions (m- and i-RegC) identified by RegCFinder. For comparison, log2 fold-changes for the WT vs. mock comparison from **Fig 1a** are also shown. Each row represents the results for one of the input windows included in **Fig 1a**. Colored rectangles on top indicate the time-point of infection or whether the original WT vs. mock comparison is shown. Statistically significant differential regions are colored according to the log2 fold-change determined by DEXSeq. Here, the color scale is continuous between -1 and 1, and all log2 fold-changes >1 are colored the same red, and all log2 fold-changes <1 the same blue. Promoter windows are ordered as in **Fig 1a**, and clusters are annotated by colored and numbered rectangles on the left. **(b)** Number of statistically significant differential regions (m- and i-RegC) and number of genes with at least one statistically significant differential region identified for each time-point of infection in the ATAC-seq time-course data. **(c)** Boxplot showing the distribution of gene expression (FPKM) values in chromatin-associated RNA for mock and 8 h p.i. WT infection for genes with significant changes in chromatin accessibility in promoter windows (i) at 4 h p.i. or earlier, (ii) at 6 h p.i. but not yet at 4 h p.i., (iii) at 8 h p.i. but not yet at 6 h p.i. and (iv) in the analysis shown in **Fig 1a**, but not yet at 8 h p.i. in the time-course ATAC-seq experiment. P-values for Wilcoxon rank sum tests comparing FPKM values in mock infection between subsequent groups are also indicated. **(d-f)** Metagene curves of ATAC-seq profiles in mock infection (red) and all time-points of infection (blue shades) from the time-course experiment, for example, clusters 5 (pattern I, **d**), 7 (pattern II, **e**) and 13 (pattern III, **f**). The colored bands below the metagene curves indicate the percentage of genes having an i- or m-RegC (blue or red, respectively) at that position in the comparison of 8 h p.i. to mock

infection from the time-course experiment. Metagene plots for all clusters are shown in **Sup. Fig 21** in **S1 File**.

Fig 5: Chromatin accessibility changes upon ICP4 knockout and dox-induced combined ICP22 and ICP27 expression

(a-b) Metagene curves showing average ATAC-seq profiles in promoter windows for mock (red), WT (blue), WT+PAA (green) and ΔICP4 (violet) infection for clusters 5 **(a)** and 7 **(b)**. Metagene plots for all other clusters are shown in **Sup. Fig 23** in **S1 File**. **(c)** Heatmap showing the location of differential regions (m- and i-RegC) identified by RegCFinder for T-HF-ICP27 cells and T-HF-ICP22/ICP27 cells upon dox exposure. Each row represents the results for one of the input windows included in **Fig 1a**. Promoter windows are ordered as in **Fig 1a** and clusters are annotated as colored and numbered rectangles on the left. Log2 fold-changes for differential regions are shown in **Sup. Fig 24b** in **S1 File**. **(d-e)** Metagene curves showing average ATAC-seq profiles in promoter windows for T-HF-ICP22/ICP27 cells with (blue) and without (red) dox exposure for clusters 5 **(d)** and 7 **(e)**. The colored bands below the metagene curves indicate the percentage of genes having an m-RegC (red, decreased upon dox exposure) or i-RegC (blue, increased upon dox exposure) or at that position. Metagene plots for all clusters are shown in **Sup. Fig 24** in **S1 File**.

Fig 6: HSV-1 infection and depletion of Pol II from human genes lead to a downstream shift of H2A.Z-containing +1 nucleosomes.

(a) Heatmap showing the location for differential regions (m- and i-RegC) identified in the WT vs. mock comparison on the ATAC-seq (left half, identical to left-most part of **Fig 1a**) and H2A.Z ChIPmentation data (right half) for the promoter windows included in **Fig 1a.** Differential regions with mock>infection (m-RegC) are marked in red, and differential regions with infection>mock (i-RegC) in blue. The order of promoter windows is the same as in **Fig**

1a, and clusters are indicated by colored and numbered rectangles on the left. Log2 fold-changes for differential regions are shown in **Sup. Fig 25b** in **S1 File**. **(b,c)** Read coverage in a ±3.6 kb window around the TSS in H2A.Z ChIPmentation data for mock (red) and WT (blue) infection, for example, genes with **(b)** pattern I (FBXO28) and **(c)** pattern II (ARHGAP1). For descriptions of read coverage plots, see caption to **Fig 1**. **(d-g)** Metagene plots of H2A.Z profiles for mock and WT infection **(d,e)** and untreated and α-amanitin-treated HCT116 cells **(f,g)** for clusters 5 (pattern I, **d,f**) and 7 (pattern II, **e,g**). Metagene plots for other clusters can be found in **Sup. Fig 25** and **27** in **S1 File**, respectively. The colored bands below the metagene curves in each panel indicate the percentage of genes having m- or i-RegC at that position. For **(f,g)**, m-RegC (green) are differential regions with relative read coverage higher in untreated cells and i-RegC (violet) differential regions with relative read coverage higher upon α-amanitin-treatment.

Fig 1

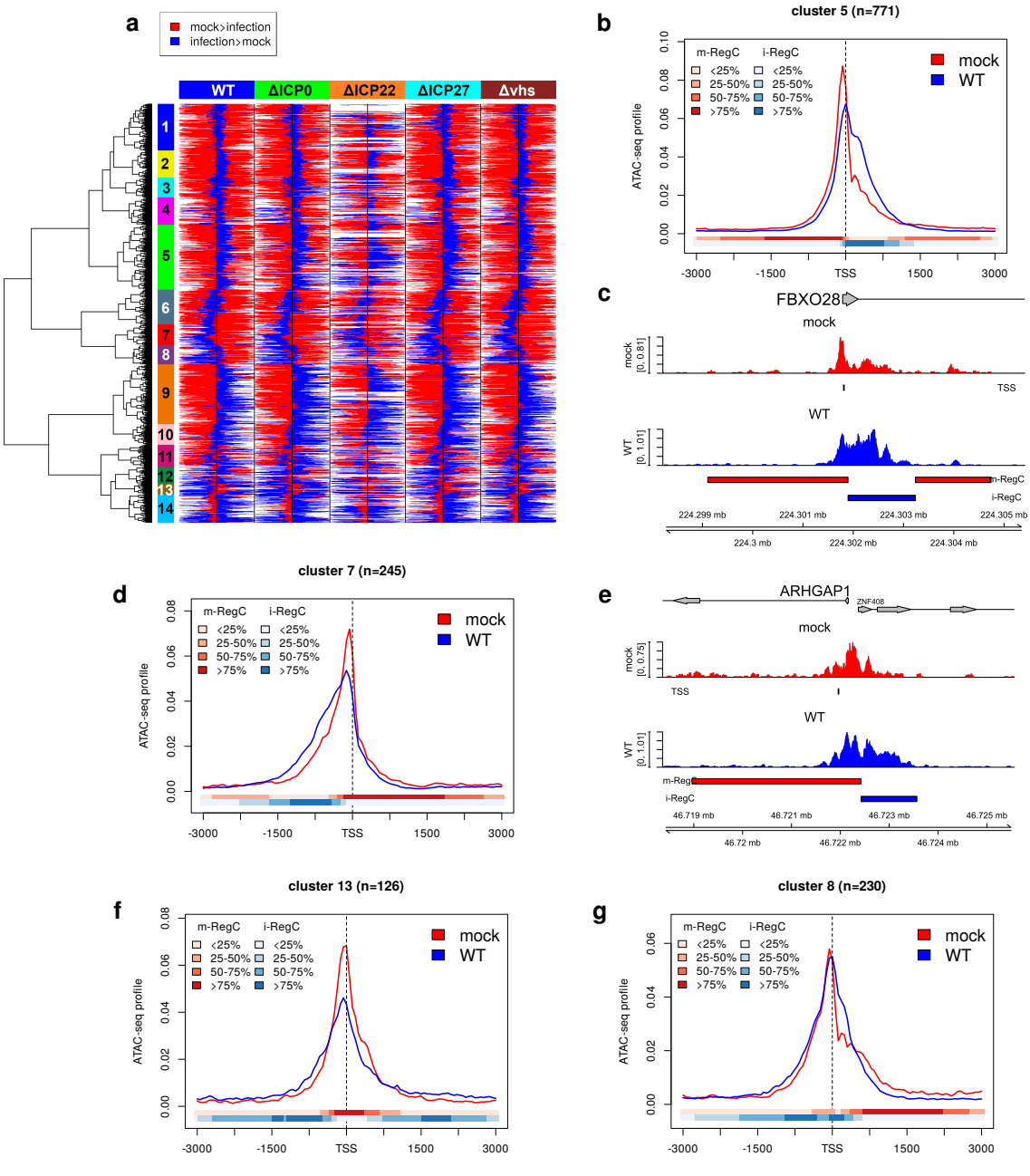
a
mock>infection
infection>mock
WT
ΔICP0
ΔICP22
ΔICP27
Δvhs
1
2
3
4
5
6
7
8
9
10
11
12
13
14
b
cluster 5 (n=771)
m-RegC
i-RegC
<25%
25-50%
50-75%
>75%
mock
WT
ATAC-seq profile
-3000
-1500
TSS
1500
3000
c
FBXO28
mock
WT
TSS
m-RegC
i-RegC
224.299 mb
224.301 mb
224.303 mb
224.305 mb
224.3 mb
224.302 mb
224.304 mb
d
cluster 7 (n=245)
e
ARHGAP1
ZNF408
46.719 mb
46.721 mb
46.723 mb
46.725 mb
46.72 mb
46.722 mb
46.724 mb
f
cluster 13 (n=126)
g
cluster 8 (n=230)

Fig 2

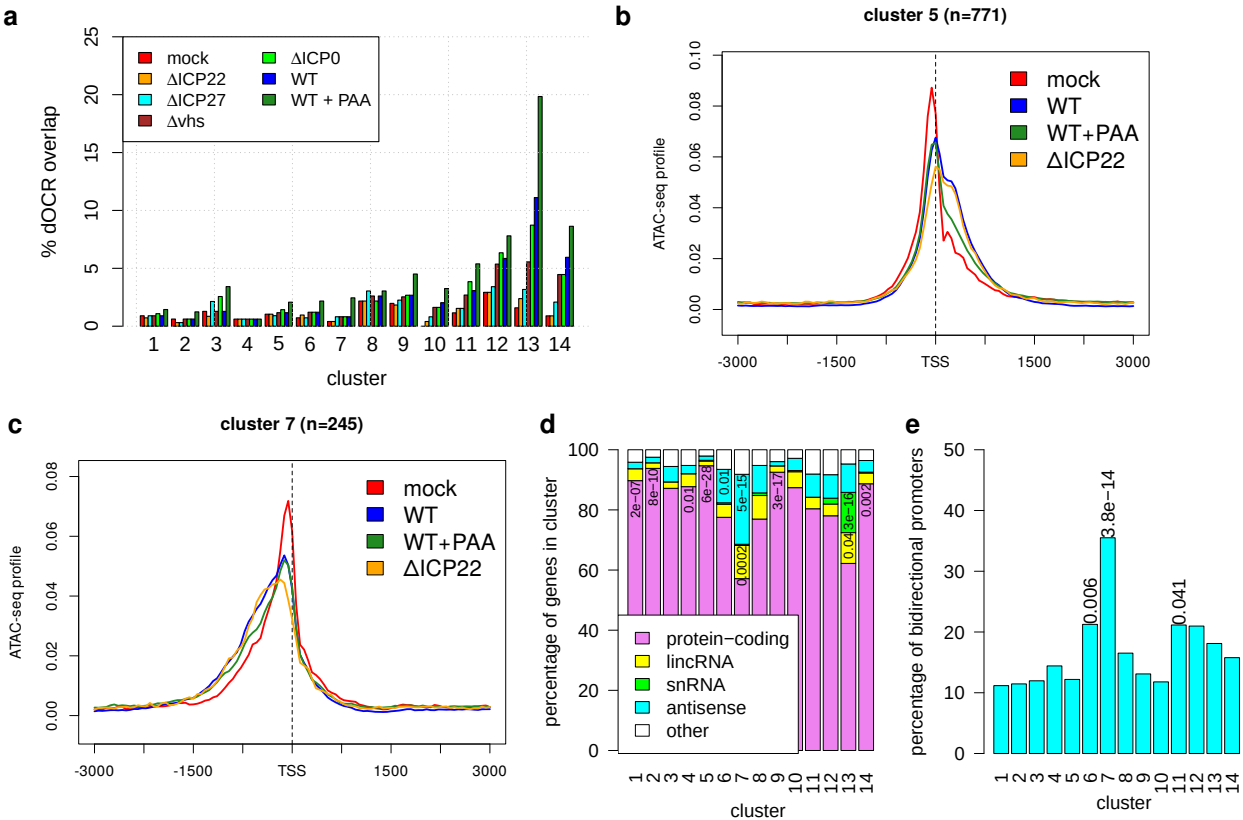
a
% dOCR overlap
cluster
mock
ΔICP22
ΔICP27
Δvhs
ΔICP0
WT
WT + PAA
b
cluster 5 (n=771)
ATAC-seq profile
TSS
mock
WT
WT+PAA
ΔICP22
c
cluster 7 (n=245)
ATAC-seq profile
TSS
mock
WT
WT+PAA
ΔICP22
d
percentage of genes in cluster
cluster
protein−coding
lincRNA
snRNA
antisense
other
e
percentage of bidirectional promoters
cluster

Fig 3

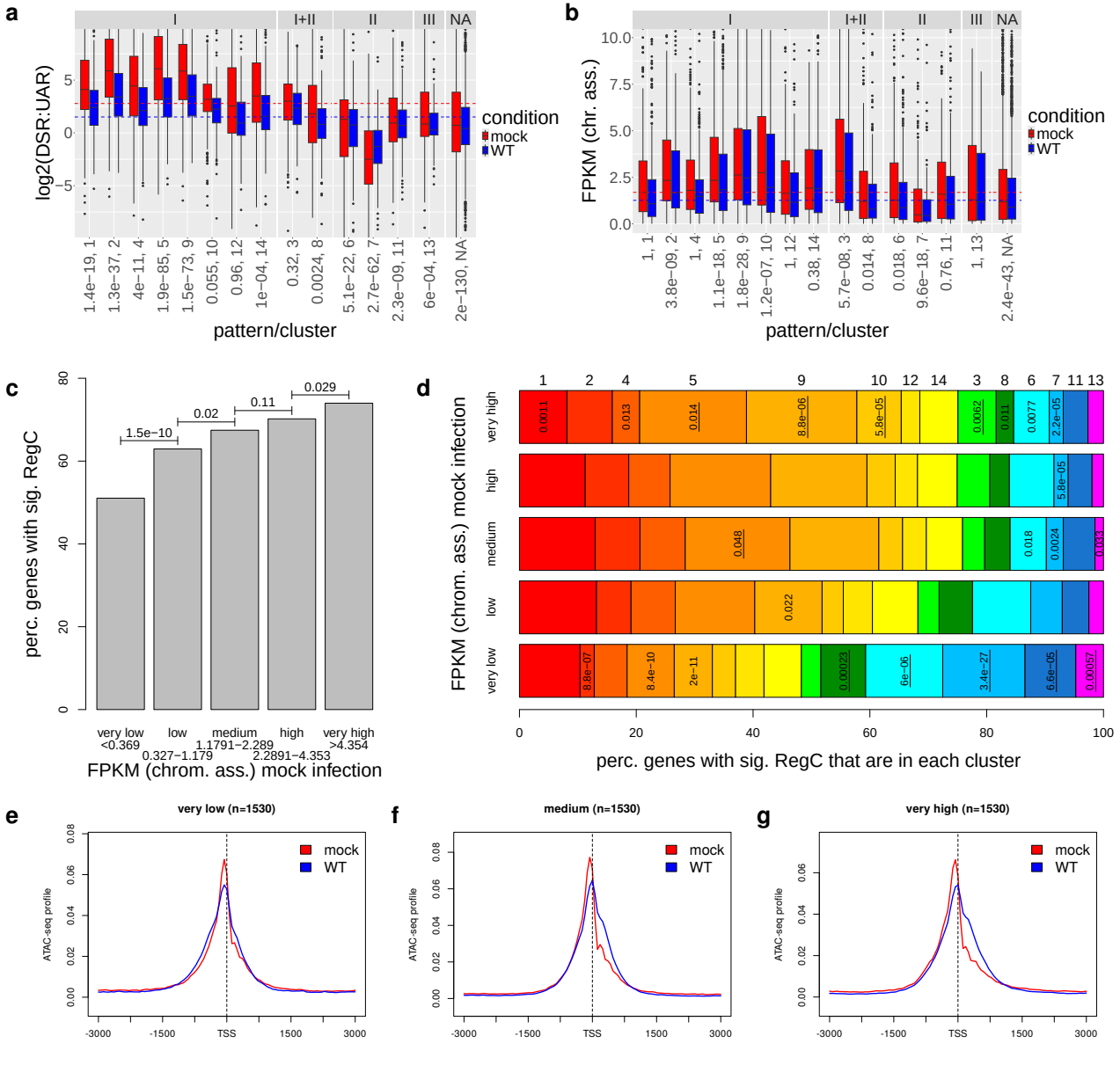
a
I
I+II
II
III
NA
log2(DSR:UAR)
condition
mock
WT
1.4e−19, 1
1.3e−37, 2
4e−11, 4
1.9e−85, 5
1.5e−73, 9
0.055, 10
0.96, 12
1e−04, 14
0.32, 3
0.0024, 8
5.1e−22, 6
2.7e−62, 7
2.3e−09, 11
6e−04, 13
2e−130, NA
pattern/cluster
b
FPKM (chr. ass.)
1, 1
3.8e−09, 2
1, 4
1.1e−18, 5
1.8e−28, 9
1.2e−07, 10
1, 12
0.38, 14
5.7e−08, 3
0.014, 8
0.018, 6
9.6e−18, 7
0.76, 11
1, 13
2.4e−43, NA
c
perc. genes with sig. RegC
1.5e−10
0.02
0.11
0.029
very low <0.369
low 0.327−1.179
medium 1.1791−2.289
high 2.2891−4.353
very high >4.354
FPKM (chrom. ass.) mock infection
d
FPKM (chrom. ass.) mock infection
very high
high
medium
low
very low
perc. genes with sig. RegC that are in each cluster
e
very low (n=1530)
ATAC-seq profile
TSS
f
medium (n=1530)
g
very high (n=1530)

Fig 4

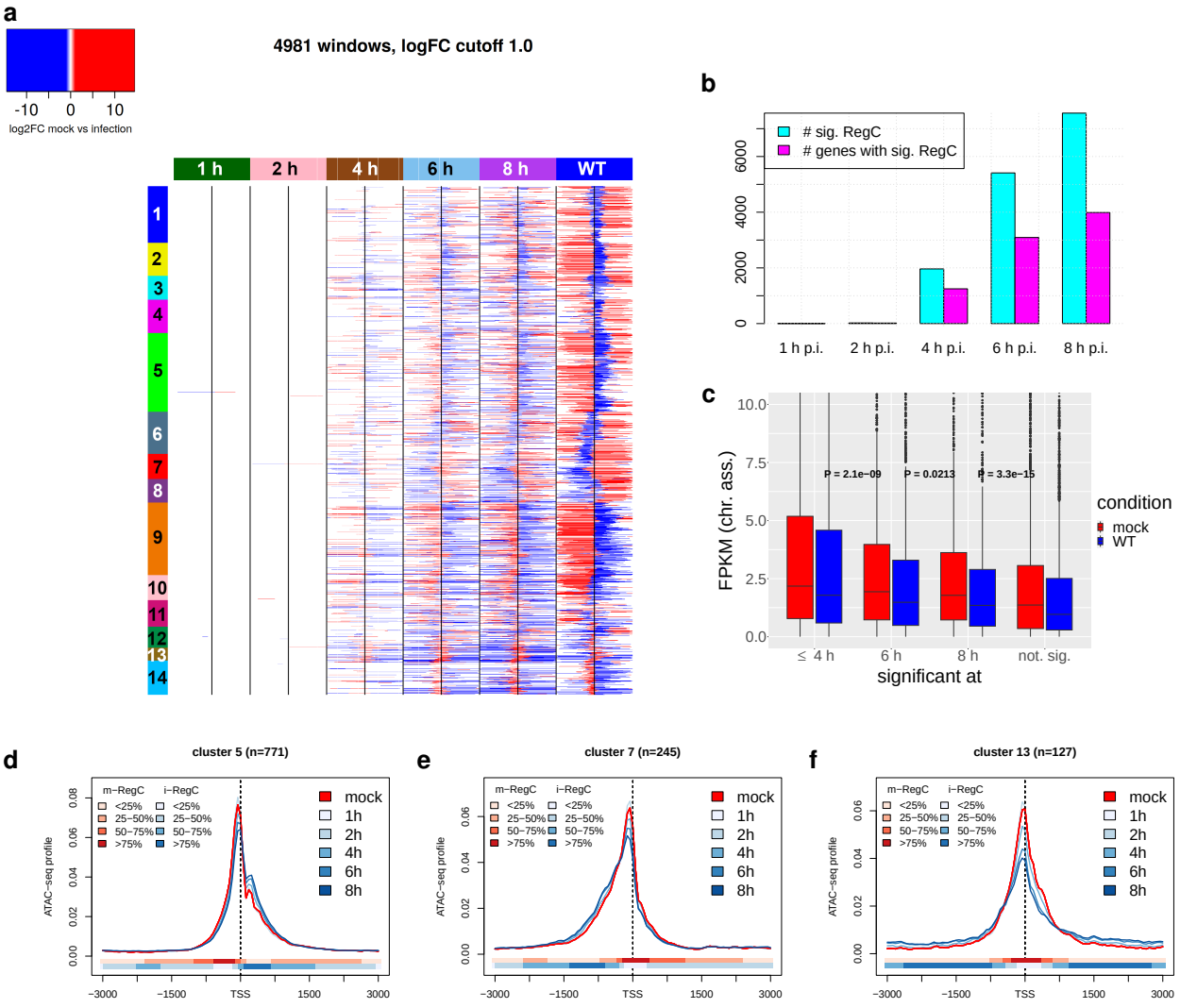
a
-10
0
10
log2FC mock vs infection
4981 windows, logFC cutoff 1.0
1 h
2 h
4 h
6 h
8 h
WT
1
2
3
4
5
6
7
8
9
10
11
12
13
14
b
sig. RegC
genes with sig. RegC
0
2000
4000
6000
1 h p.i.
2 h p.i.
4 h p.i.
6 h p.i.
8 h p.i.
c
FPKM (chr. ass.)
10.0
7.5
5.0
2.5
0.0
P = 2.1e−09
P = 0.0213
P = 3.3e−15
≤ 4 h
6 h
8 h
not. sig.
significant at
condition
mock
WT
d
cluster 5 (n=771)
e
cluster 7 (n=245)
f
cluster 13 (n=127)
ATAC−seq profile
m−RegC
i−RegC
<25%
25−50%
50−75%
>75%
mock
1h
2h
4h
6h
8h
−3000
−1500
TSS
1500
3000

Fig 5

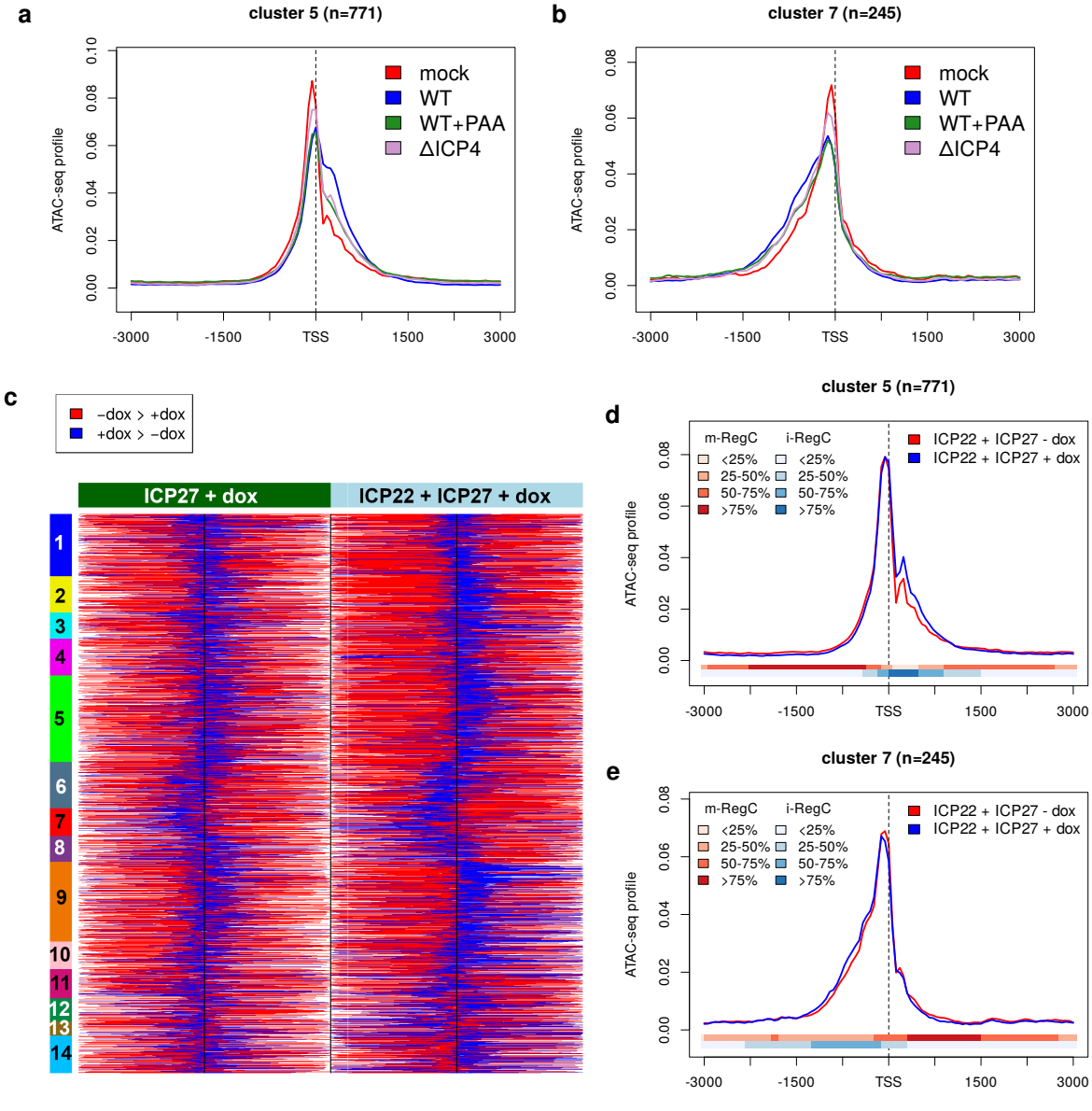
a
cluster 5 (n=771)
ATAC-seq profile
mock
WT
WT+PAA
ΔICP4
-3000
-1500
TSS
1500
3000
b
cluster 7 (n=245)
c
−dox > +dox
+dox > −dox
ICP27 + dox
ICP22 + ICP27 + dox
d
cluster 5 (n=771)
m-RegC
i-RegC
<25%
25-50%
50-75%
>75%
ICP22 + ICP27 - dox
ICP22 + ICP27 + dox
e
cluster 7 (n=245)

Fig 6

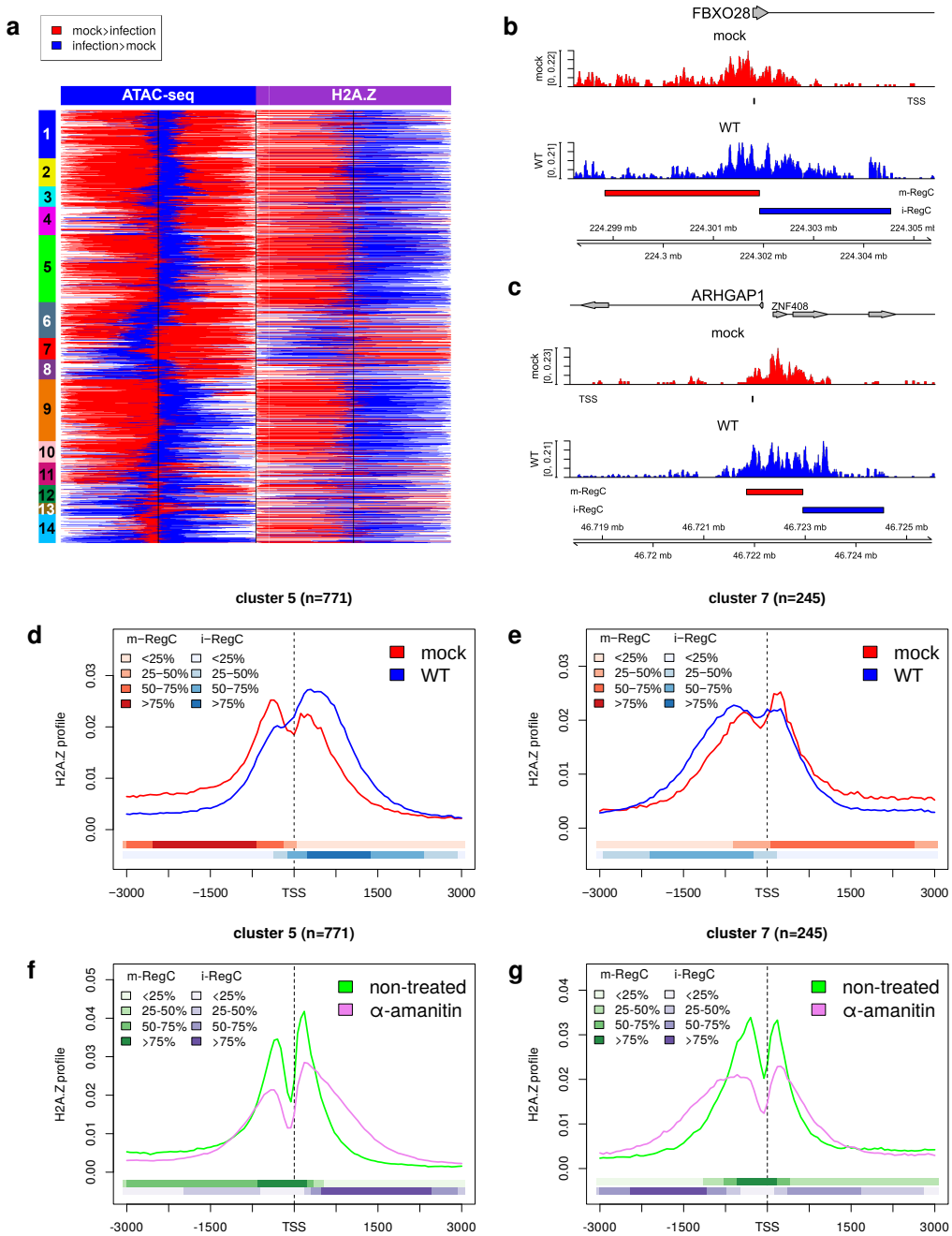
a
mock>infection
infection>mock
ATAC-seq
H2A.Z
1
2
3
4
5
6
7
8
9
10
11
12
13
14
b
FBXO28
mock
mock
[0, 0.22]
TSS
WT
WT
[0, 0.21]
m-RegC
i-RegC
224.299 mb
224.301 mb
224.303 mb
224.305 mb
224.3 mb
224.302 mb
224.304 mb
c
ARHGAP1
ZNF408
mock
mock
[0, 0.23]
TSS
WT
WT
[0, 0.21]
m-RegC
i-RegC
46.719 mb
46.721 mb
46.723 mb
46.725 mb
46.72 mb
46.722 mb
46.724 mb
cluster 5 (n=771)
d
m−RegC
i−RegC
<25%
25−50%
50−75%
>75%
mock
WT
H2A.Z profile
0.00
0.01
0.02
0.03
−3000
−1500
TSS
1500
3000
cluster 7 (n=245)
e
m−RegC
i−RegC
<25%
25−50%
50−75%
>75%
mock
WT
H2A.Z profile
0.00
0.01
0.02
0.03
−3000
−1500
TSS
1500
3000
cluster 5 (n=771)
f
m-RegC
i-RegC
<25%
25-50%
50-75%
>75%
non-treated
α-amanitin
H2A.Z profile
0.00
0.01
0.02
0.03
0.04
0.05
-3000
-1500
TSS
1500
3000
cluster 7 (n=245)
g
m-RegC
i-RegC
<25%
25-50%
50-75%
>75%
non-treated
α-amanitin
H2A.Z profile
0.00
0.01
0.02
0.03
0.04
-3000
-1500
TSS
1500
3000